Scale-up of Continuous Chemical Synthesis Systems

by

Patrick Louis Heider

B.S. Chemical and Biological Engineering, Rensselaer Polytechnic Institute, 2007
M.S. Chemical Engineering Practice, Massachusetts Institute of Technology, 2009

Submitted to the Department of Chemical Engineering
in partial fulfillment of the requirements for the degree of

Doctor of Philosophy in Chemical Engineering
at the
MASSACHUSETTS INSTITUTE OF TECHNOLOGY

September 2013

Author_____
Department of Chemical Engineering
July 1, 2013

Certified by_____
Klavs F. Jensen
Warren K. Lewis Professor of Chemical Engineering
Professor of Materials Science and Engineering
Thesis Supervisor

Accepted by_____
Patrick S. Doyle
Chairman, Committee for Graduate Students

Scale-up of Continuous Chemical Synthesis Systems

by

Patrick Louis Heider

Submitted to the Department of Chemical Engineering on July 1, 2013
in partial fulfillment of the requirements for the degree of
Doctor of Philosophy in Chemical Engineering

Abstract

Continuous flow systems for chemical synthesis have become increasingly important in the pharmaceutical and fine chemical industry in the past decade. Initially, this work was confined primarily to microfluidic systems, but recently there has been a growing demand for milliscale systems capable of making material for clinical trials and pilot plant testing. The objective of this thesis is to demonstrate a practical system to accomplish continuous chemical synthesis within the context of a fully integrated pilot plant. The plant provided a platform to test scaled-up membrane-based liquid-liquid separators which were studied in detail.

Previous work demonstrated the use of microfiltration membranes to separate liquid-liquid systems by leveraging the dominance of interfacial tension over gravity at small scales. When scaling up, it was determined that pressure control was critical to the operation of the separators. A pressure control module was designed and integrated into the separator device to provide the appropriate conditions to guarantee separation. The separators required no outside control to accomplish separation when connected to various downstream conditions including pumps, backpressure controllers, and other separators. This allowed for easy design and operation of multistep processes such as solvent swaps and countercurrent extraction.

The main accomplishment covered in this thesis is the building and operation of an integrated continuous manufacturing plant for a small molecule pharmaceutical product (aliskiren tablets). An advanced intermediate was continuously processed through two synthetic steps with workup which are detailed here. The remainder of the process purified and formulated the drug substance and formed the final tablet which met many key performance criteria.

This work opens avenues to look at even more complex liquid-liquid and even gas-liquid separation processes. Improved processes for continuous manufacturing which make use of recycling, multistage extraction, and novel chemistries can build on the research performed here to further improve synthesis systems. These results demonstrate that continuous processes are possible even for complex, industrially-relevant products.

Thesis Supervisor: Klavs F. Jensen
Title: Department Head, Chemical Engineering
Warren K. Lewis Professor of Chemical Engineering
Professor of Materials Science and Engineering.

Acknowledgements

I would first like to thank Professor Jensen for the opportunity to work in his lab. I came to MIT not entirely sure what I wanted to do and he showed me a project with some mention work that would relate to actual industrial problems. Little did I know that would lead me down the path of building an entire pilot plant. He gave me tremendous freedom to work on this project and basically disappear for a year while we were building and running the plant. I have greatly benefited from his guidance and support whenever I encountered a difficulty – technical or otherwise.

This work would not have been possible without the generous funding of Novartis. They came to us 6 years ago with an incredibly challenging problem and then let us struggle with it until we were able to finally succeed. They showed incredible foresight and trust to allow us to keep working on the pilot plant, even in the face of setbacks and delays. I am especially grateful to Markus Krumme and Berthold Schenkel who provided invaluable insights from their perspective on the relative industrial merits of our work.

The Jensen group of researchers has been an amazing group of people to work with. They made coming to work each day enjoyable with many great conversations and insights. I want to especially thank Hemant Sahoo for helping orient me in the lab and get me going when I had no idea how to build microfluidic systems. I had several excellent UROPs work for me over the years. Lucy Ji stands out for her extended dedication to a difficult project. I am also indebted to Ryan Hartman and Stephen Born. Ryan shared valuable insight into managing projects which proved to be critical to jumpstarting the pilot plant project. Stephen was always willing to help whether it was a chemistry question or exercising training question. The last year of my work was highlighted by collaboration with Andrea Adamo on two projects. He is an amazing person who brought many critical design insights and also a great support personally. Lastly, I would not have made it through grad school without Jason Moore. He was always willing to listen when things were falling apart and somehow was able to put up with sharing an apartment my entire time at MIT.

I was fortunate to be able to be able to work with two groups, the second being the “Red Line” team. Headed by James Evans, this group was a wonderful group to share so many challenges with. The many, many long nights (and days) running the pilot plant created a lot of stress, yet everyone on the team still gave 100 % and were a pleasure to work with. The pilot plant team also allowed me the opportunity to work with a number of extremely talented and hardworking Northeastern University coop students. They brought an energy and motivation to the project which was unmatched by any of the MIT researchers. Aaron Wolfe and Louis Buchbinder, the first two I worked with, merit additional thanks. They joined the project at an especially difficult point and provided invaluable assistance the semester I was TAing. Richard Lakerveld provided many helpful insights into research and was the bedrock of the plant during operation by monitoring everything at the control system station. I was also fortunate to work with Michael Hogan from Siemens setting up the pilot plant. He was more of a MIT grad student than most of the students I work with. Lastly, I want to thank Sal Mascia and Haitao Zhang. They were the only team members, amidst a constant turnover of short term and partial time

members, who stay on the project as long as me. We grew to know each other extremely well and could eventually troubleshoot things with each other with barely saying a word. I am happy to call them friends.

The support of friends and family has been constant during my time at MIT. Seth Sibley provide a much needed refuge away from MIT in western Mass to escape on weekends. Steven Morris has provided great perspective and laughter as a friend in grad school elsewhere. My friends who play floorball have introduced me to a great sport that always reminds me that no matter how much I am running around like an idiot at work, it is nothing compared to playing floorball. Lastly, and most importantly, I owe a massive debt to my brother and parents. Tom has always been willing to share his perspective and act as a role model on how to handle grad school without losing yourself. Finally, my parents were the best support system I could ask for. They would listen when I needed it, and push me along when I needed encouragement. I owe this thesis to them.

Table of Contents

List of Figures

List of Tables

List of Schemes

Chapter 1. Introduction, motivation, and objectives

1.1 Introduction and motivation

1.1.1 Microfluidic flow chemistry

Flow chemistry has been growing in prominence since microfabrication techniques were applied to create channels for fluid flow in the late 1990s.[1] Since then, there have been numerous papers written in the organic chemistry field demonstrating improved performance for certain reactions in flow and expanding the chemical space available to flow. Initially, interest in microfluidics centered on performing reactions that are difficult to run in conventional batch glassware.[2, 3] Common examples include taking advantage of the higher heat transfer and small amounts of reagents required in microfluidic devices. Researchers have run highly exothermic reactions at room temperature rather than chilled to low temperatures[4] or reactions that pose safety hazards when run at larger scales in batch.[5] While initially of interest only to engineers, flow chemistry has been more widely adopted by chemists in both academia[6] and industry.[7]

The current field of flow chemistry has matured and now many reactions have been demonstrated in flow, both reactions that perform better in flow and those that are currently better in batch. One analysis of relevant chemical transformations found that half of the reactions typically performed would be improved by operating in flow.[8] The authors point out that of those reactions, over 60 % involve solids which have traditionally posed problems for flow chemistry, especially in microreactors. This highlights the new direction flow chemistry is going – towards solving how to perform problematic transformations in flow. Already there is work showing how to handle solids in flow for some reactions involving solids.[9]

Kirschning[6] identified ten issues which flow chemistry can address specifically the last two of which are of particular importance to this thesis: multistep synthesis and scale-up. Performing multiple steps in one device was a goal of many early researchers in the field (Figure 1).[10-12] While many of these early systems were more feats of engineering by combining reactions, pumping, analysis, and more on a single, monolithic device, more recent work has used more modular systems.[13] This provides the opportunity to reconfigure the system and perform other types of transformations and allow the wider chemical space to be tested in flow systems. Modern microfluidic systems more resemble the chemical plants of the commodity

chemical industry with separate, distinct unit operations connected by pipes/tubes (Figure 2). By performing multiple reaction steps in series, it becomes more difficult to avoid transformations that are difficult or suboptimal in flow. Roberge and coworkers[8] determined that the average production campaign involves 2.1 reaction unit operations. Therefore in order to be industrially relevant, flow processes should include multiple steps and be able to connect them together without isolations to remain truly continuous.

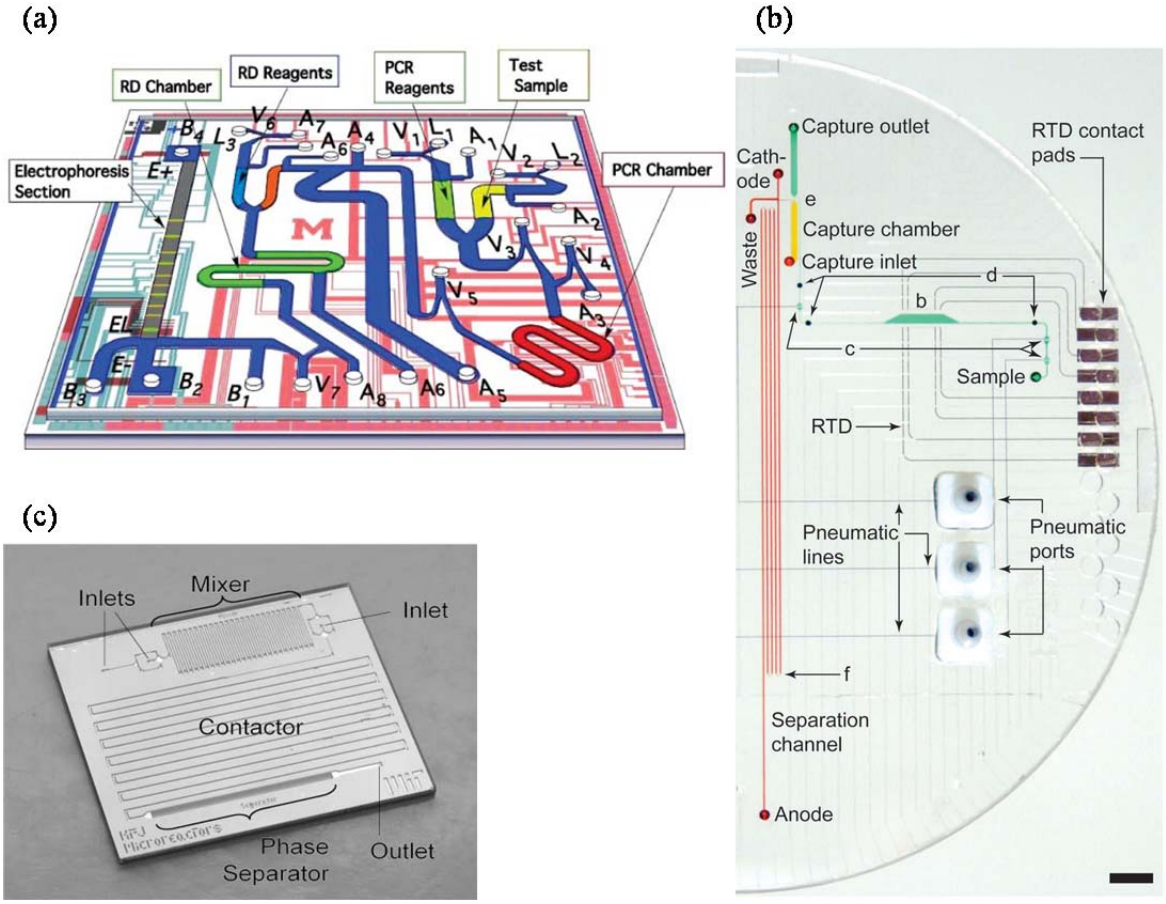

Figure 1. Multistep flow processes on a chip for (a) genetic analysis of influenza,[11] (b) DNA sequencing,[12] and (c) liquid-liquid extraction.[14]

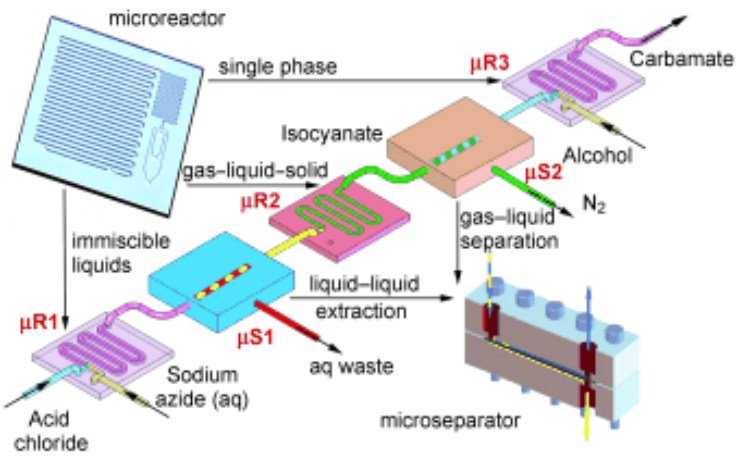

Figure 2. Microfluidic multistep synthesis process incorporating several unit operations.[15]

The workup steps in a chemical process, although not often considered as important as the reaction steps, are actually more numerous (2.7 workup steps compared to 2.1 reaction steps).[8] One key workup step used in most synthetic routes is liquid-liquid extraction. Typically, gravity is used as the driving force to separate the two phases; however, at small length scales, the interfacial forces are much higher. Previously, researchers have shown that selectively wetting membranes can accomplish separation between the two liquid phases by leveraging the capillary force in the membrane pores.[14] When scaling up to the milliscale, it is less clear what separation strategy provides the best performance. Membrane separators have been scaled up using the same principles at microscale and milliscale, but they have required additional control of the pressure on the outlets to maintain separation (Figure 3a).[16] Centrifuges increase the apparent gravity force felt by the fluids and can be operated continuously (Figure 3b).[17, 18] They are also a common unit operation found at larger scales and do not require additional control beyond the initial set up of the separation chamber. One major drawback is the centrifuge itself is fairly complex and therefore expensive compared to other separation devices. Lastly, settling tanks can be used to separate two liquid phases (Figure 3c).[19, 20] While these devices are very simple, they can require large volumes to separate fluids of similar densities or emulsions. They also require some form of control to maintain the two liquid levels.

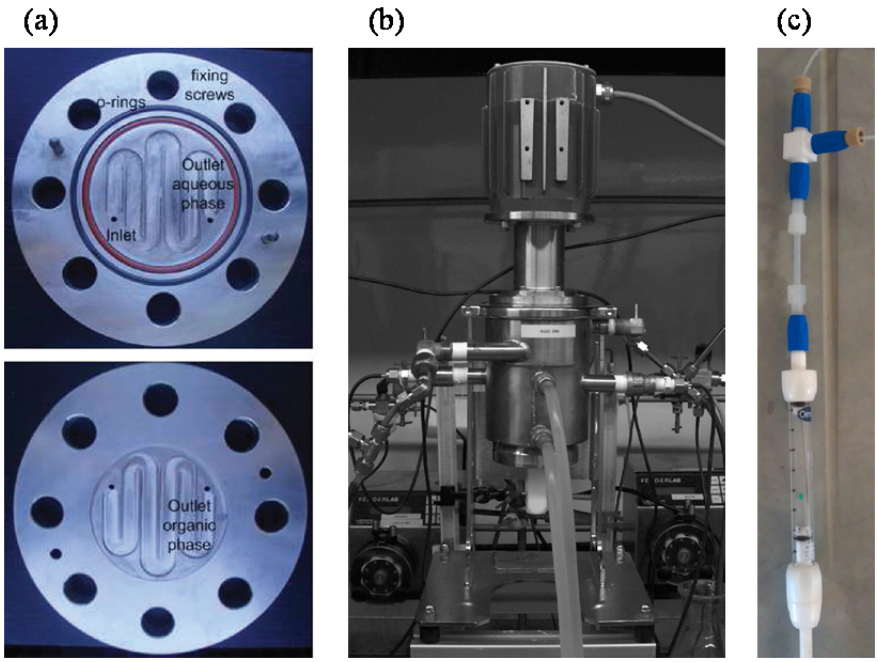

Figure 3. Various milliscale liquid-liquid separators: (a) membrane based separator opened with membrane removed;[16] (b) continuous centrifugal separator;[18] (c) settling tank with float interface detection[20]

1.1.2 Continuous manufacturing in the pharmaceutical industry

The pharmaceutical industry has experienced massive economic pressure over the past 5-10 years. While the loss of blockbuster drugs is a significant contributor to these concerns, the cost to research and develop a new pharmaceutical has also been implicated as a point of concern as well.[21, 22] The number of new drugs registered for development with the FDA (new molecular/chemical entities, NME's) has remained relatively flat, the cost to develop the drug has been growing at an increasing rate (Figure 4). This has drawn attention to the research and development divisions of pharmaceutical companies as potential areas for cost savings. During the heyday of blockbusters, the manufacturing costs were negligible and therefore the groups responsible for development and scale-up could operate with little scrutiny or recognition. The early 2000s saw a shift with many companies beginning to show increased interest in R&D. The entire R&D process has been highlighted now as a critical step in the process of bringing a product successfully from early research and lead identification to full scale manufacturing.[23, 24]

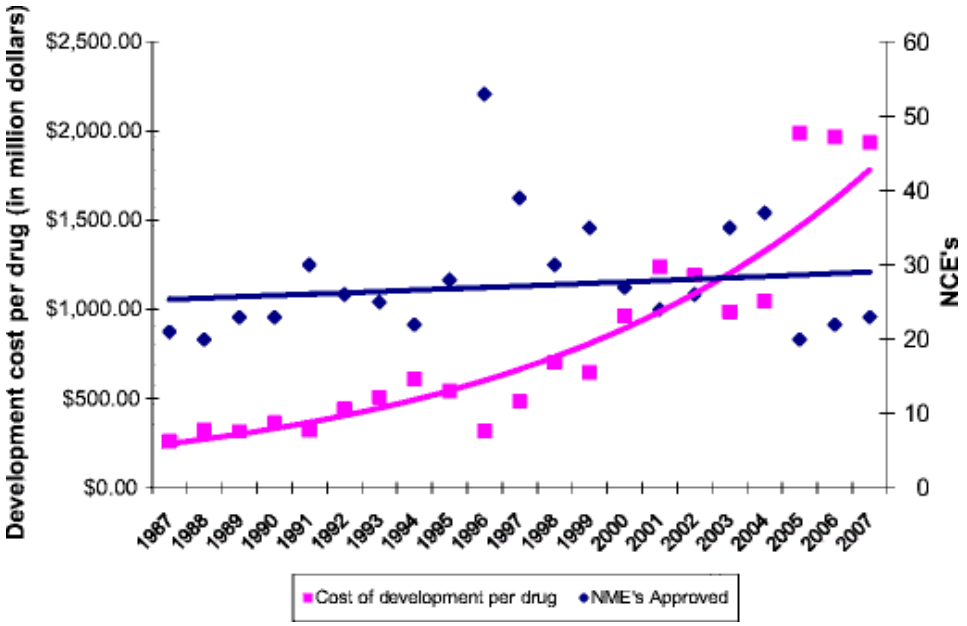

Figure 4. Estimated development cost per drug and number of new chemical/molecular entities registered over time.[22]

More so than other chemical industries, the pharmaceutical industry's R&D branches are concerned with operating their processes at multiple scales. The commodity chemical or petrochemical industry would test a process on a bench scale in manual glassware then possibly scale up once to a pilot plant before quickly going to full scale depending on how well understood the process is. The various scales would make enough product to test that it meets specification, but generally the demand for material only exists once production scale is achieved. The pharmaceutical industry operates under a completely different paradigm. R&D units are constantly making batches of material to support safety and clinical trials (Figure 5). As the product moves along development process, batches get larger as more material is required; however, there is a much smoother curve of processes at various scales. This highlights the specific need in the pharmaceutical industry to not only have processes that operate at many scales, but to simplify the changes between scales so unexpected product failures which would hold up clinical trials do not occur.

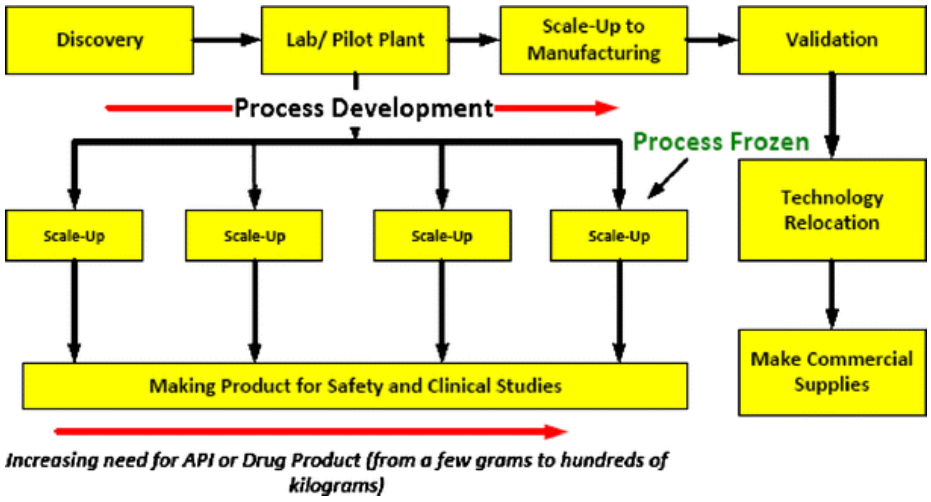

Figure 5. Process R&D in the pharmaceutical industry[22]

The growing focus on process development within the pharmaceutical industry coinciding with the increased interest in flow chemistry soon saw a convergence with many pharmaceutical companies looking into how continuous manufacturing could improve their process development and manufacturing.[25] This interest has extended beyond the concept of cost to improved process quality, safety, and environmental impact.[26] There is widespread agreement that there are still many challenges to overcome before continuous manufacturing will be adopted widely by the pharmaceutical industry. A general lack of understanding how these processes would work is still present, although it is improving as more examples of continuous processes are detailed.[27] A lack of commercial processing equipment, especially at the milliscale required for later clinical trials where the process must be locked down before final scale-up to pilot and production. To this point, the only continuous manufacturing processes are confined to either upstream chemical synthesis or downstream formulation/formation, but there is interest in fully integrated processes from synthesis to final product. Two major issues that are not addressed in this thesis, but still deserve mention, are the presence of existing batch capacity and uncertainty regarding FDA regulation of continuous processes.

1.2 Thesis objectives

The main objective of this thesis is to extend the previous work on flow chemistry performed at the microscale to milliscale, multistep systems. Specifically, this is done in the context of a fully integrated, continuous pilot plant. This plant provides an industrially relevant

example to test the concepts of continuous manufacturing and highlight the areas where new technologies are required. One piece of technology specifically addressed in this thesis is liquid-liquid separation. The controlling physics are elucidated and used to develop design and scale-up equations for the separator. Examples of enabled multistep processes are provided to demonstrate the simple use of the separators to complex systems.

The pilot plant itself has a set of objectives regarding the full integration of all unit operations and producing a final product that meets commercial quality standards. Offline holding and isolations are avoided such that the plant is a truly continuous process. This requires designing operating points to be robust to disturbances and amenable to automated control as only limited buffering capacity is available to handle disruptions. Insights into heuristics and techniques that facilitate the design and operation of continuous pharmaceutical processes are highlighted.

1.3 Thesis outline

Chapter 2 describes in detail the design and operation of the membrane-based liquid-liquid separators. The key design parameters as well as scale-up criteria are provided. A novel, integrated differential pressure controller which effectively decouples the separator from downstream units is demonstrated. This new device is tested to validate the design parameters and show applications in multistep separations such as solvent swaps and countercurrent extraction.

Chapter 3 provides a general overview of the continuous pilot plant built to produce tablets containing the small molecule pharmaceutical aliskiren. A high level overview of the process is given along with some results on the general operation of the plant. The key performance criteria for the plant are detailed and the quality of the final drug product is examined.

Chapter 4 details the reaction and workup steps in the pilot plant. The development of the chemical reactions as well as the modeling and design of the full scale process is presented. A detailed look at the long term performance during a 10 day run is presented to validate the chosen design.

Chapter 5 summarizes the conclusions from this thesis as well as offering some promising directions for future work.

Appendix A is a highly detailed description of the final pilot plant design. It also has an in depth discussion of the online concentration measurements used in the pilot plant. Appendix B examines the content uniformity performance criteria of the final tablets in more detail. Lastly, Appendix C contains the design drawings for a scaled-up membrane-based separator used in the continuous pilot plant.

Chapter 2. Membrane-based, liquid-liquid separation with integrated pressure control

2.1 Introduction

The last decade has seen a growing effort in the development of continuous flow chemical systems ranging from microscale[1, 3, 6, 13, 28-30] to milliscale.[18, 31-35] The field has expanded in scope beyond single reactor and synthesis steps to multistep synthesis including intermediate workup and separation steps.[15, 16, 36-39] Among the separation techniques available to organic chemists, liquid-liquid separations are becoming more popular.[40] The small length scales encountered in continuous systems on the microscale and milliscale improve the extraction rate due to higher mass transfer coefficients,[41, 42] but present challenges for separation as surface forces dominate over the traditionally used gravity force.[43] Several solutions have reported including parallel flow,[44-46] settling tanks,[19, 20] selectively wetting channels,[47-49] centrifugation,[17, 18] and microfiltration membranes.[14, 16] All of these separation techniques (except settling tanks and centrifugation) rely on the interfacial tension, γ, between the two liquids to provide the force to achieve separation.

Previous studies have demonstrated capillary pressure, P_{cap}, is a critical parameter which must be balanced with other forces in the device to guarantee proper operation of a separator.[16, 47, 50] P_{cap} is given as

$$P_{cap} = \frac{2\gamma\cos(\theta)}{r} \tag{1}$$

where θ is the contact angle between the solid material of the device and two liquid phases and r is the radius of curvature of the interface. The design of each system is such that P_{cap} must be higher than the pressure difference across the interface, or separation will be incomplete. Since γ and θ are material properties that vary for each application, the only available design parameter is r which must be minimized to produce stable operation. In microscale systems, this is easy to do in a single channel with a small gap for parallel flow or two selectively wetting channels. Milliscale systems require larger channels to keep the pressure drop small relative to P_{cap} and therefore need many smaller channels to maintain high P_{cap} while permitting high flow rates.

This is easily achieved using microfiltration membranes.[14, 16] Membrane-based separators are therefore ideal candidates for operating at both microscale[15] and milliscale.[16]

Previous analyses of membrane-based separators have focused on the importance of balancing the flow resistances through each outlet[14] or pressure control of individual outlets.[16, 47] These design criteria produce functioning devices; however, they make integration into larger systems difficult as downstream fluctuations can easily disrupt separation. A solution to this problem has been the use of break tanks and additional pumps[15] which increases the volume and complexity of the systems. Break tanks with additional pumps can be eliminated by careful design for specific operating conditions at the cost of flexibility and robustness. Direct control of the pressure at the separator outlets can also avoid break tanks,[16] but still requires a feedback loop to account for differences in operating conditions downstream.

This chapter reexamines the governing equations for separation in a membrane-based separator and presents a new separator design with an integrated pressure control component. The new design decouples the unit from downstream operations, increases flexibility, and eliminates the necessity for feedback control. Easy to implement solvent swap and countercurrent extraction examples are presented.

2.2 Design theory

There are two main failure modes for membrane-based separators. The first is breakthrough of the retained phase which occurs when the pressure drop across the membrane (transmembrane pressure, ΔP_{mem}) is greater than P_{cap}. The second failure mode is when the permeate phase is partially retained by the membrane and exits with the retained phase. This occurs when there is insufficient pressure to cause the permeate liquid to flow through the membrane (P_{per}) which can be approximated by

$$P_{per} = \frac{8\mu Q_p L}{n\pi r^4} \tag{2}$$

where μ is the viscosity of the permeate phase, Q_p is the entering permeate liquid volumetric flow rate, L is the membrane thickness, n is the number of pores and r is the pore radius. This assumes that the membrane acts as an array of cylindrical pores which is acceptable for this analysis as shown below. A third failure mode exists where two phase streams exit both outlets,

but this is indicative of operating the separator at a flow rate excessive for the available membrane area and therefore this condition is generally not encountered.

When the pressure drop along the length of the membrane channel is negligible compared to $P_{cap} - P_{per}$, then these two failure modes can be described in a single compound inequality

$$P_{cap} > \Delta P_{mem} > P_{per} \tag{3}$$

since ΔP_{mem} can be assumed to be constant along the membrane. This assumption is satisfied when the channel is sized so that pressure drops along its length are negligible. The first inequality is satisfied by appropriate selection of the membrane (material and pore size) while the second is better understood by replacing ΔP_{mem} with $P_1 - P_2$ where P_1 is the pressure on the retentate side of the membrane and P_2 is the pressure on the permeate side of the membrane and rewriting as

$$P_{cap} + P_2 > P_1 > P_{per} + P_2 \tag{4}$$

Equation (4) means that successful designs must always operate under conditions where the retentate pressure is some value greater than the sum of the permeate pressure and the P_{per} value for the maximum flow rate desired through the membrane.

Figure 6 shows a schematic of the membrane separator which incorporates a pressure control segment immediately following the membrane. The pressure control is made up of a diaphragm stretched over the retentate stream with the permeate stream flowing on the reverse side. Since the diaphragm seals against the retentate flow path, no flow exits the retentate side of the separator unless $P_1 > P_2$. Additionally, the membrane is slightly deformed conveying an additional force on the retentate flow path that must be exceeded to permit flow. This device then acts as a differential pressure controller such that $P_1 = P_{dia} + P_2$ where P_{dia} is the additional pressure due to the tension on the diaphragm. This simplifies Equation (4) to

$$P_{cap} > P_{dia} > P_{per} \tag{5}$$

which means that an appropriately designed separator will achieve complete separation as long as the flow rate through the membrane remains below maximum value for the design (that is pressure drops along channels are negligible).

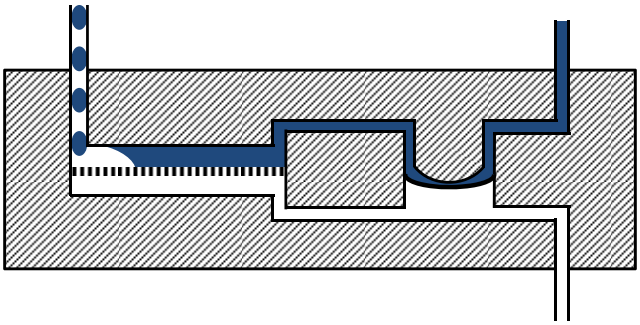

Figure 6. Integrated pressure control in membrane separator showing deformed diaphragm (heavy curved line) to provide a fixed pressure difference across the membrane (short vertical lines). The aqueous and organic phases are shown in blue and white respectively.

2.2.1 Scale-up of membrane separators

As membrane separators increase in scale, the pressure drop, P_{chan}, along the length, l, of the channel increases. This is depicted graphically in Figure 7. The value for P_{chan} can be approximated by

$$P_{chan} = \frac{8\mu\left(Q_p + Q_r\right)l}{\pi R^4} \tag{6}$$

where Q_r is the retained liquid flow rate and R is the channel radius (for a circular channel). Equation (6) and Figure 7 provide a conservative estimate as the pressure drop along the permeate side is assumed to be 0 while the pressure drop on the retentate side is approximated by the total flow rate of both phases. In the actual system, the retentate side flow rate will decrease, reducing the pressure drop while the permeate side will have some pressure drop, both of which will reduce the ΔP_{mem}. This gives rise to an additional constraint on operation of the membrane separators given in Equation (7).

$$P_{chan} < P_{cap} - P_{dia} \tag{7}$$

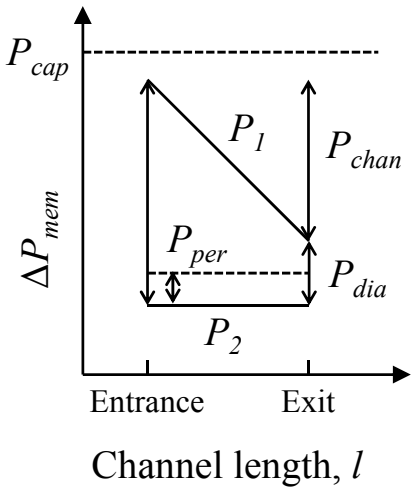

Figure 7. Simplified diagram of pressure values in membrane-based separator

As the scale of the separator increases (increasing Q_p), the geometry of the separator must be changed to keep similar performance. Performance is characterized by maintaining similar pressures such that similar absolute pressure fluctuations and relative flow rate fluctuations can be tolerated. One simple way to solve scaling up, especially for tube membranes is to scale-out the number of channels in a single shell in a hollow fiber membrane module. This requires distribution across many channels of the two phase incoming stream which will become difficult once the geometry becomes large enough for gravity to become significant and cause settling of the two phases. Alternatively, the geometry of a single fiber can be adjusted by examining

$$\frac{2\gamma\cos(\theta)}{r} = P_{cap} > P_{dia} > P_{per} = \frac{4\mu Q_p L}{\hat{n}\pi^2 r^4 l R} \tag{8}$$

and

$$P_{chan} = \frac{8\mu(Q_p + Q_r)l}{\pi R^4} < P_{cap} - P_{dia} \tag{9}$$

where $\hat{n}$ is the specific pore density (pores area^{-1}). As Q_p increases, eventually the second inequality in Equation (8) will be violated. This can be avoided by increasing R proportionally. Alternatively, the value of l can also be increased but eventually the inequality in Equation (9) will be violated unless $R^{1/2}$ is increased proportionally as well. This will allow the separators to be scaled up until the point when gravity becomes significant in the tube resulting in a change in the flow profile. The lighter phase will move to the top of the channel and the effective

membrane area will decrease as permeate slugs no longer contact the whole membrane. Increasing both l and $R^{1/2}$ will allow for a larger maximum Q_p before this affect becomes significant.

Rectangular channels with flat membranes on the top or bottom surfaces require a slightly different analysis. The relevant equations for a single sided membrane separator, as is currently used, are

$$\frac{2\gamma\cos(\theta)}{r} = P_{cap} > P_{dia} > P_{per} = \frac{8\mu Q_p L}{\hat{n}\pi r^4 wl} \tag{10}$$

and

$$P_{chan} = \frac{K\mu(Q_p + Q_r)l}{wh^3} < P_{cap} - P_{dia} \tag{11}$$

where w is the channel width (parallel the membrane, perpendicular to flow), h is the channel height (perpendicular to flow and the membrane), and K is a constant which depends on the ratio of w and h.[51] In order to compensate for increases in Q_p, the value of w can be increased proportionally or the value of l can be increased which also increasing either $h^{2/3}$ or w^2. Increasing w indefinitely would introduce distribution issues for the entering two phase stream. By increasing l, the membrane can be coiled into a spiral wound membrane module. In this case, two, opposite sides of the channel would be made of membrane material changing the right most expression in Equation (10) by a factor of 0.5. If l is increased, then increasing h is a better choice for maintaining similarity on scale-up. Since both sides of the channel are made of membrane material, even if the height increases enough to allow gravity to settle the two phases, the permeate phase will still remain in contact with the membrane. The efficiency will be lower as not all of the membrane will be wetted with the permeate phase, but separation would still occur as long as the efficiency drop is not enough to require too much additional length for membrane area.

2.3 Experimental section

Figure 8 shows a photograph of a separator constructed out of polycarbonate. Better chemical compatibility was provided by constructing the separator out of high molecular weight polyethylene (HDPE). The membranes used were Pall Zefluor 1 μm PTFE microfiltration

membranes which are wet by the permeating organic phase and retain the aqueous phase with a total area of 290 mm^2. The diaphragm was made of PFA film with a thickness of 25 μm and 50 μm. The 25 μm film provided a smaller pressure difference, but was prone to damage so the thicker film was used which was more robust but provided a higher pressure difference. All pumping was performed using piston pumps from Knauer (Smartline pump 100), Eldex (Optos 2SIP), and Fuji Techno Industries (Super metering pump HYM-08).

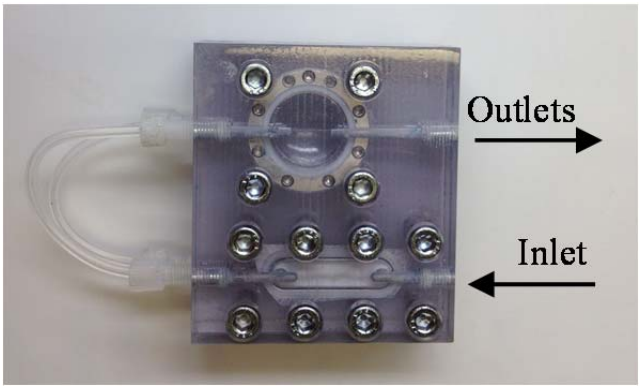

Figure 8. Photograph of polycarbonate membrane separator with integrated pressure control. The separator membrane is located on the lower portion and the pressure control diaphragm is located on the upper portion of the device.

The design equations were tested by removing the loops connecting the separation membrane with the differential pressure controller and attaching 235 cm of 1.6 mm inner diameter (ID) tubing to the permeate outlet and 60 cm of 0.76 mm ID tubing and 183 cm of 1.6 mm ID tubing to the retentate outlet. Previously contacted and separated water and ethyl acetate were each pumped at 5 mL/min into a tee mixer and then passed into the membrane separator. Pressure variations across the membrane were controlled by varying the height of the outlets over 2 m and calculating the pressure at the membrane. Failure points were calculated using Equation (3). The values for R and L were taken from the manufacturer's specifications and n was calculated by measuring the membrane flow resistance by flowing only toluene and measuring the flow rate split between the two outlets. The value of γ was taken from the literature[52] as 36.1 mN/m for toluene-water and 6.8 mN/m for ethyl acetate-water. The differential pressure controller was tested by measuring the flow rate split between the two

outlets when flowing only toluene through the device. 50 cm of 0.51 mm ID tubing was added to increase the pressure drop on the permeate side of the membrane so that flow exits both outlets.

Characterization of the new separator design where the membrane is coupled to the pressure controller was done following the set up represented in Figure 3. Hexane-water and ethyl acetate-water pairs were tested. The first one provided an initial test bed for the system with a wide operating range due to a high interfacial tension (50 mN/m), the second was a more challenging separation as the interfacial tension between the two fluids is an order of magnitude lower (6.8 mN/m) thus restricting the pressure difference operating window for successful separation. Ratios of flow rates from 4:1 to 1:1 were tested with each stream varying between 2 and 8 mL/min. Additionally to test the robustness of the pressure controller, the pressure in the collection reservoir of the organic side was changed to apply backpressure to the separator simulating downstream pressure drop (0, 1, 1.4, and 2 bar were used).

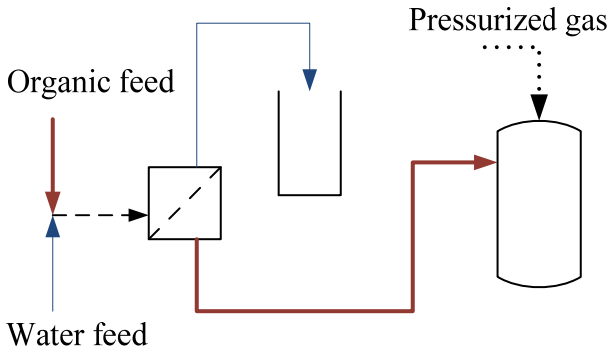

Figure 9. Setup for testing of membrane separator with integrated pressure control. Organic phase lines are shown in dark red, water lines are shown in blue, and two phase streams are shown as dashed lines. The organic outlet of the separator entered a closed vessel pressurized by a gas.

2.3.1 Solvent swap

A two stage solvent swap was tested as shown in Figure 10. A stream of 0.34 M benzoic acid in ethyl acetate was pumped at 1 mL/min into a mixing tee to contact a stream of 0.55 M NaOH flowing at 1 mL/min. A HDPE separator then split the phases with the organic phase passing through the membrane and through an additional 0.6 bar backpressure controller. This was added because the organic outlet of the separator generally must be at a higher pressure than

the aqueous or else excess pressure on the aqueous outlet (in this case due to the second separator) will cause breakthrough of the aqueous phase by overriding the differential pressure controller. The aqueous phase containing benzoic acid then contacted a 1 mL/min stream of toluene. After a short length of tubing, a 1 mL/min stream of 0.6 M HCl was added. The stream was then separated by a second, identical membrane separator. Tubing with lengths to provide > 10 s of residence time was used to allow the streams to reach equilibrium prior to separation. All tubing used was 1.6 mm ID. The flow rate of each outlet stream was measured by collection in graduated cylinders and the concentration of benzoic acid determined by HPLC (Agilent 1100 with UV detector, 30 mM H_3PO_4 aqueous mobile phase, and 1:1 acetonitrile:methanol organic mobile phase). The results were compared to a comparable batch extraction performed at a 50 mL scale in separatory funnels with careful measurement of volumes.

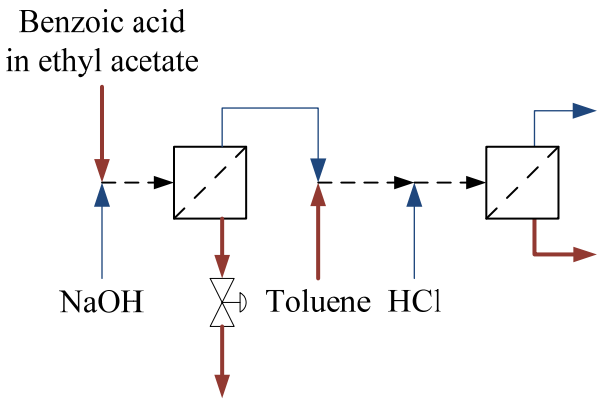

Figure 10. Flow diagram of solvent swap setup. Organic phase lines are shown in dark red, water lines are shown in blue, and two phase streams are shown as dashed lines.

2.3.2 Countercurrent extraction

A three stage countercurrent extractor was set up as shown in Figure 11. Toluene and water were used as solvents with acetone as the extractant added at a 0.05 mass ratio to either solvent. The toluene feed was pumped by a single pump while a separate aqueous phase pump was used at each stage to increase the pressure so countercurrent operation was possible. All pumps were set to 3 mL/min. All tubing was 0.76 mm ID PFA with sufficient lengths to allow equilibrium before separation at each stage (residence time > 5 s). The outlet flow rates were measured and the concentration of acetone was determined by HPLC (Agilent 1100 with RI

detector and 5 mM H_2SO_4 isocratic mobile phase) for the aqueous phase and GC (HP 6890 with FID detection) for the organic phase. Samples were taken after 15 min of operation with 3-5 repeats over the first hour. Performance was determined using standard countercurrent extraction plots.[53]

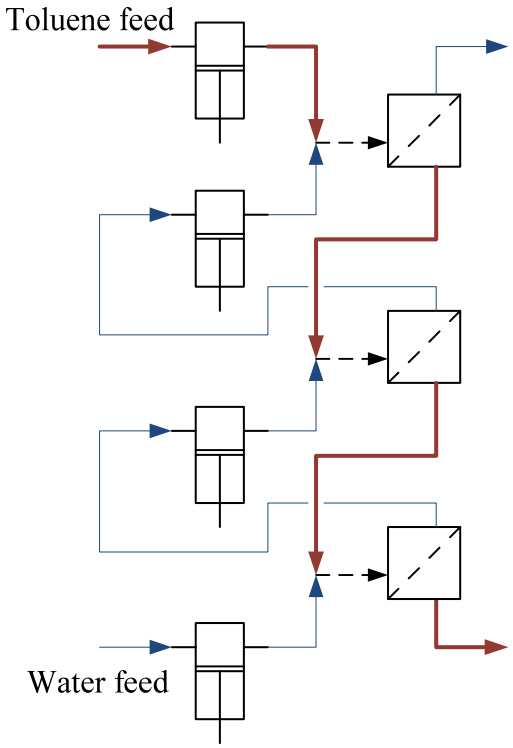

Figure 11. Flow diagram of countercurrent extraction setup. Organic phase lines are shown in dark red, water lines are shown in blue, and two phase streams are shown as dashed lines.

2.4 Results and discussion

The initial design of the separator was tested to confirm the assumptions from the theory section above held for the separator. The separator was operated without the differential pressure controller at 5 mL/min with a 1:1 ethyl acetate-water system. The results shown in Figure 12 compare the model predictions of the flow rate out the permeate side of the membrane with experimental results for varying ΔP_{mem}. While the performance of the separator is qualitatively similar to the model, breakthrough of the aqueous phase happens at much lower ΔP_{mem} values. This is indicative of a pore size distribution where a small number of pores with larger radii allow the aqueous phase through while the other pores still prohibit flow. The large flat region shows that the design parameters described above can be used to select an appropriate P_{dia} for

the differential pressure controller to allow separation by operating below the calculated P_{cap}. Figure 13 shows that the differential pressure controller performance across a wide range of flow rates is fairly constant and within an acceptable range for most applications. The values of P_{cap} for both the toluene/water and ethyl acetate/water systems and the values of P_{per} for each flow rate bound the values for P_{dia} meaning the separator satisfies Equation (5) and should separate effectively.

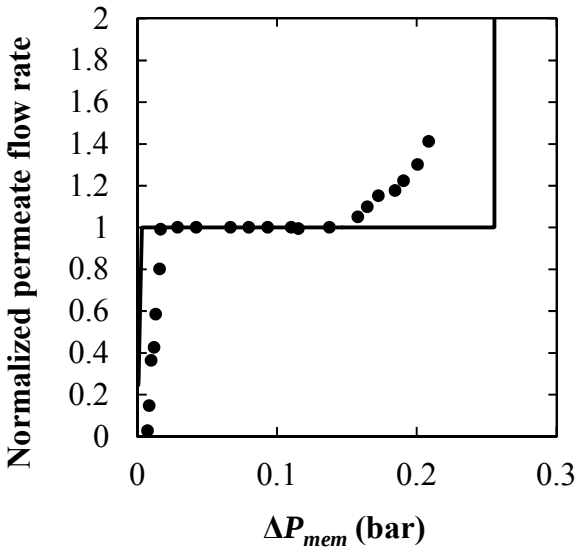

Figure 12. Plot of model and experimental results of the membrane separator without pressure control. The flow rate through the permeate outlet normalized by the inlet organic flow rate is plotted verses ΔP_{mem} where a value of 1 means perfect separation. Model values are given by the solid line while experimental values are given by circles. A flow rate of 5 mL/min was used for each phase.

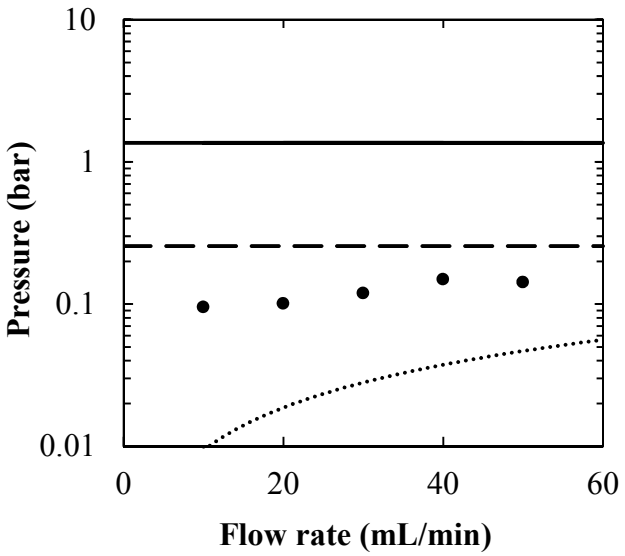

Figure 13. Plot of the differential pressure controller's performance, P_{dia}, versus flow rates (circles). The solid and dashed lines represent P_{cap} for a toluene-water and ethyl acetate-water separation respectively. The dotted line represents P_{per} for each flow rate. The separator meets the criteria of Equation (5) for all flow rates.

Results from the testing of the operation of a single separator with the integrated pressure controller are shown in Table 1. The table shows that as back pressure increases, a modest breakthrough can be observed for the ethyl acetate-water pair. This can be interpreted in light of the results of Figure 12 and Figure 13. Figure 12 shows that the ethyl acetate-water system begins to allow breakthrough of the aqueous phase at 0.15 bar while Figure 13 shows that P_{dia} was between 0.1 and 0.15 bar for single phase flow. High pressures applied to the organic outlet cause small deviations in the performance of the pressure control diaphragm, slightly increasing P_{dia} which was sufficient to cause some breakthrough in the ethyl acetate-water system. Importantly, the hexane-water system has a sufficiently high P_{cap} that the small increase in did not cause any failure in separation across all the conditions tested.

Table 1. Summary of performance of a membrane separator with integrated pressure control

	Aqueous flow rate mL/min	Organic flow rate mL/min	Normalized permeate flow rate[a] Backpressure on organic outlet 0 bar	1 bar	1.4 bar	2 bar
Hexane-water	2	2	1	1	1	1
	5	5	1	1	1	1
	8	8	1	1	1	1
	2	8	1	1	1	1
	8	2	1	1	1	1
Ethyl acetate-water	2	2	1	1	1.0425	1.0500
	5	5	1	1.0108	1.0384	1.0930
	8	8	1	1.0159	1.0476	1.1180
	2	8	1	1	1.0625	1.2420
	8	2	1	1.0213	1.0492	1.0123

[a]The flow rate through the permeate outlet is normalized by the inlet organic flow rate (where 1 is perfect separation).

2.4.1 Solvent swap

The ability to change solvents between successive synthesis steps ('solvent swap') is an important consideration in using optimum solvent choices for the individual reactions. As a demonstration case, the separator was tested in a two stage solvent swap of benzoic acid from ethyl acetate to toluene. The results of the extraction are summarized in Table 2. The continuous system reproduces the batch performance both in terms of yield and mass balance. The system was operated for 2 h without any failure in the separation and requiring no additional control beyond starting each pump up sequentially (the first stage pumps, then the second stage pumps). This application demonstrated how the separator effectively decouples the membrane pressures from effects downstream when the pressure on the organic outlet is greater than the aqueous outlet. The 0.6 bar of backpressure on the first stage permeate (organic) outlet would normally prevent flow without the presence of the differential pressure controller, but the pressure controller increased the pressure on the retentate side by enough to force only the organic phase through. This is similar to the effect when a separator is used to separate an organic phase which contains the reactant for a subsequent reaction. Normally increased pressure required for a second reactor (to increase the boiling point of a solvent or due to a fixed bed) would require additional pressure control on the retentate (aqueous) side to closely match the organic pressure.

The differential pressure controller simplifies the system by negating the need for the retentate side pressure control.

Table 2. Summary of solvent swap results comparing a batch shake flask and continuous with two membrane separators

	Yield[a]	Mass balance[a]
Continuous	0.92 +/- 0.006	0.97 +/- 0.008
Shake flask	0.94	0.96

[a]Error values are one standard deviation of 4 samples taken over the 2 h run.

A similar situation existed on the retentate side of the first separator in that it fed a second separator with a differential pressure controller that elevated the pressure. The effects of this pressure on the first separator were eliminated by adding a static backpressure regulator to the permeate side of the first separator larger than the highest pressure the retentate side might see. If this was not done, the first separator will not separate at all, but after adding the fixed regulator no additional control was required as long as the retentate pressure remained below 0.6 bar. The first stage was completely isolated from the second stage such that even during startup when the second stage was not running, the first stage will separate both streams. No additional adjustments were needed to maintain separation when the second stage was started up.

2.4.2 Countercurrent extraction

The separators were also tested in a countercurrent extraction setup. This required setting up one pump for the organic phase and a pump for the aqueous phase for each stage to drive the countercurrent flow. The separator achieved three stages of extraction (Figure 14) when extracting acetone from either toluene or water. This was expected since the high mass transfer rates in slug flow[41, 42] ensured that equilibrium was achieved before separation at each stage. Since extraction and separation occur independently, this system could be scaled to a large number of stages with additional separators and pumps without any extraction efficiency issues. This is an improvement over other small scale countercurrent systems[44, 54, 55] which have a low number of stages and are limited in their flow rate by stage efficiencies related to the throughput. The decoupling of the pressure in each stage makes the setup and operation of the countercurrent separator simple. The system needed to be initially primed with solvent for each phase as the

piston pumps used could not handle two phase streams. After turning on each pump, the system then operated without any outside control for over 1 h, eliminating level control between stages for mixer/settler systems.[20]

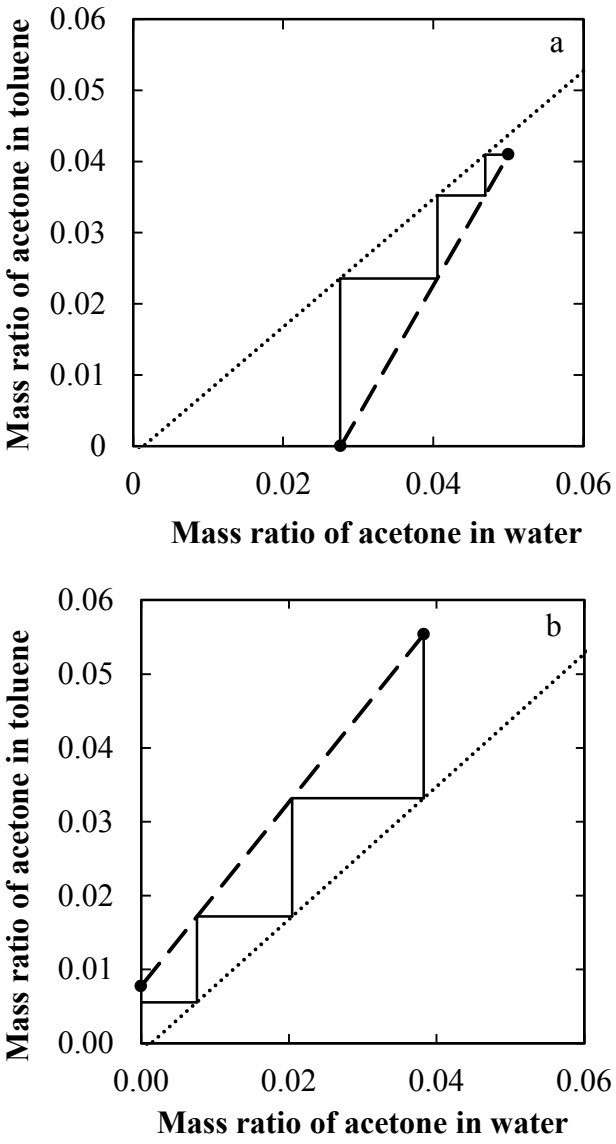

Figure 14. Extraction diagram for (a) extraction of acetone from water into toluene and (b) extraction of acetone from toluene into water. The equilibrium curve is shown by a dotted line and the operating line is shown by the dashed line; stages are stepped off with a solid line.

2.4.3 Scaled up membrane modules

Several different scaled up membrane separation devices were developed. Photos of each design are shown in Figure 15 with key parameters given in Table 3. Detailed drawings of the membrane separator designs are given in Appendix C. Each separator was installed with a 0.5 μm PTFE membrane and tested with equal flow rates of water and ethyl acetate to determine the maximum flow rate of each phase possible. No pressure control device was used when testing these designs. The values determined are approximations of the scale at which each separator operates. The initial design (Design 1) is shown in Figure 15a. This device is constructed out of PEEK to be acid resistant. It is typically used for low flow rates such as those encountered in microfluidic applications. Design 2 (Figure 15b) increased both the channel height and width to reduce the pressure drop per length while increasing the length to cover as much of the 47 mm diameter membrane as possible. To further increase the throughput, a parallelized device with 4 equal branches was created which used a 142 mm diameter membrane (Figure 15c). The specific device photographed was constructed out of ultrahigh molecular weight polyethylene. This material deformed when compressed and did not seal the membrane well resulting in leaks. It was able to separate at the highest throughput available on the pumps (80 mL/min). A compression system involving metal parts which do not deform would improve sealing the large surface area. The final design (Figure 15d) involved a sandwich design with layers of PTFE and metal caps to compress the inner polymer layers. This device also could separate at the flow rate limit of the pumps. The reason the limit was higher for Design 4 than Design 2 which had more area was the failure of Design 2 was due to pressure drop along the channel (P_{chan}) violating the first inequality in Equation (3) (P_{cap}). Design 4 had a shorter channel length reducing P_{chan} while still having sufficient membrane area permit flow of all the organic phase through the membrane, Equation (2).

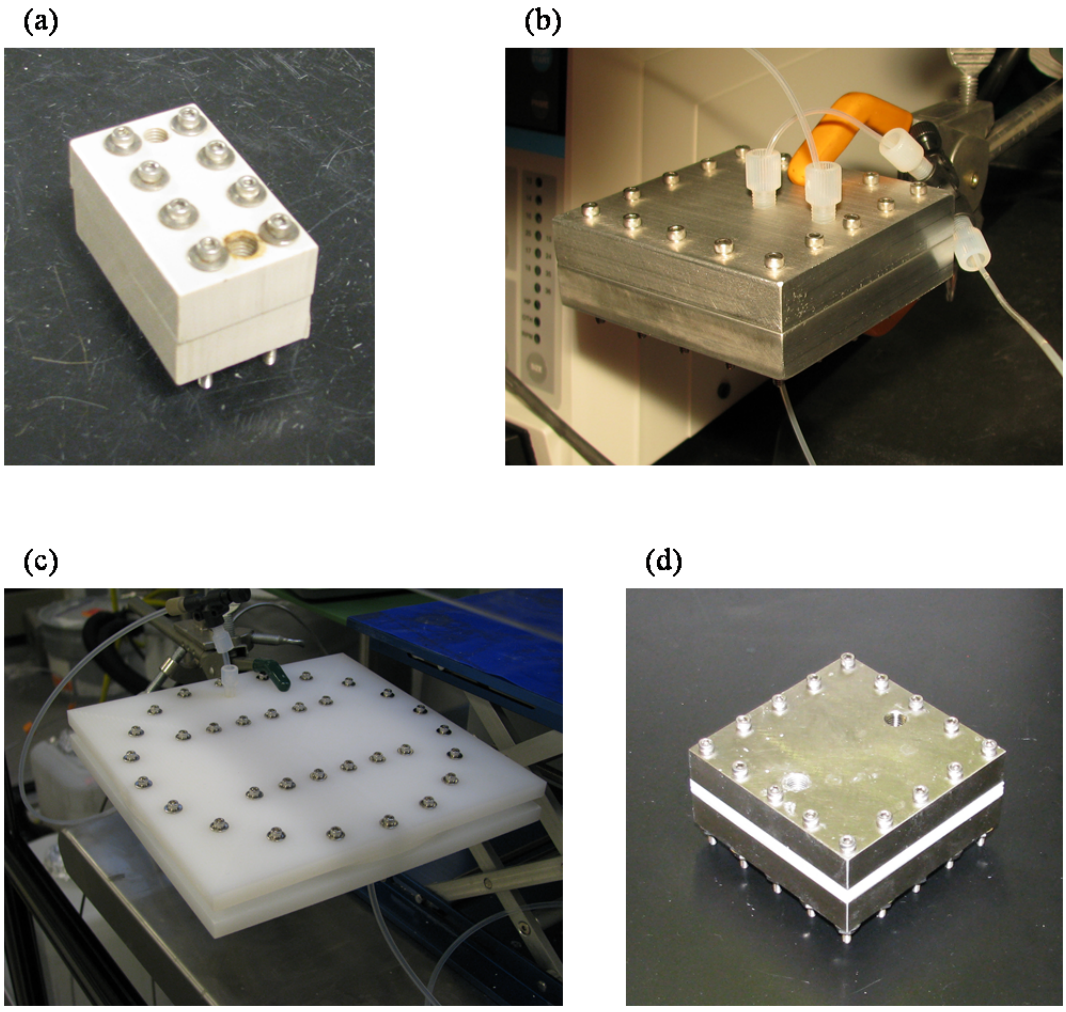

Figure 15. Scaled up membrane-based separators: (a) Design 1; (b) Design 2; (c) Design 3; (d) Design 4

Table 3. Key criteria and performance of separators

Design #	Channel height (mm)	Channel width (mm)	Channel length (mm)	Channel area (mm^2)	Max flow rate[a] (mL/min)
1	1	2.4	25.4	61	5
2	2	2	460	910	80
3	2	3	400 × 4	1200 × 4	> 80
4	1.6	3.2	270	860	> 80

[a]The maximum flow rate where complete separation occurred at equal flow rates of water and ethyl acetate using a 0.5 μm pore size PTFE membrane.

2.5 Conclusions

The membrane-based separator presented here is an advance in continuous flow separators at the milliscale. The integrated pressure controller greatly reduces the complexity when implementing separators within chemical reactor systems by decoupling the separator pressures and limiting the online control required for operation. It is the first demonstration of countercurrent multi-stage liquid-liquid extraction using membrane based separators. Further, it simplifies multistep chemical systems including reactions coupled to separation and other multistage separations such as cross flow extraction. Larger systems which incorporate dynamic control would benefit from the intrinsic pressure control since control actions which affect downstream pressures (flow rate fluctuations, composition changes, etc.) can be tolerated without redesigning the system or additional control on the separator. The separator is useful in research settings since little additional changes are required to switch the separator between different applications. Future work to scale the separator down and determine the upper limits of this design are ongoing as well as applications to more complex, multistep syntheses.

Chapter 3. End-to-end continuous manufacturing of pharmaceuticals

3.1 Introduction

The pharmaceutical industry has seen numerous pressures in the past decade to improve efficiency as rising costs outpaced the development of new pharmaceuticals.[21, 22] A growing interest in green processes also highlights areas for improvement in pharmaceutical synthesis and manufacturing where environmental impacts have been higher than other industries.[26, 56] Continuous manufacturing has attracted the attention of industry and academia alike by promising lower costs, greater reliability and safety, better sustainability, and novel pathways not otherwise accessible.[25, 57] Recent studies have demonstrated that economic savings can be realized for certain cases by transforming a batch production into continuous.[58-60] Existing batch-based manufacturing can take up to 12 months between the start of the first synthetic step and market release of finished tablets,[61] partially resulting from movement of materials around and between facilities and lengthy final product testing. This results in large, expensive inventories and shortages from manufacturing delays if the batch fails after production during final testing. Continuous manufacturing allows faster response to demand changes, which permits reduced inventory compared to batch-based manufacturing resulting in not only lower working capital, but also decreased amounts of potentially hazardous intermediates, including high potency active pharmaceutical ingredients (API). Increasing use of online monitoring and control also reduces the burden of final testing, mirroring the online control present in other continuous manufacturing industries.[62, 63] Simulations of processes that include recycle loops demonstrate improvements to process yield and robustness can be achieved by operating continuously.[64-66] While promising, there are still many hurdles for implementation of continuous processes.[6, 8, 26] These include development of flow chemistry transformations, difficulties processing dry solids and solid-laden fluids, lack of equipment at bench and pilot scale, development of control methodologies to guarantee product quality and breaks in the process especially between synthesis and formulation. The literature contains many examples of continuous processes for chemical synthesis in flow,[3, 7, 13, 37, 67-69] reactions with workup,[15, 16, 19, 27] continuous

crystallization,[27, 70-74] drying,[75-77] powder blending,[78-81] and tableting,[81-84] however, only few others have considered multistep portions of a process.[27, 81, 84, 85]

This chapter covers the first example of an end-to-end, integrated continuous manufacturing plant for a pharmaceutical product. The plant starts from a chemical intermediate and performs all the intermediate reactions, separations, crystallizations, drying, and formulation resulting in a formed final tablet in one tightly controlled process. This provides a platform to test newly developed continuous technologies within the context of a fully integrated production system and investigate the system-wide performance of multiple interconnected units. This chapter presents the key results of operating the plant for runs of up to 10 days. Specifically it highlights areas where advantages exist for continuous flow and discusses techniques relevant to continuous processes.

3.2 Process overview

The target API is aliskiren hemifumarate (Scheme 1, **6**) formulated as tablets containing 112 mg of aliskiren free base, **5**. The total throughput of the plant is nominally 45 g h^{-1} of **6** corresponding to 2.7×10^6 tablets y^{-1}. The throughput can be adjusted by changing control setpoints in the plant between 20 g h^{-1} and 100 g h^{-1}. The plant layout is compact with a 2.4 m × 7.3 m footprint entirely contained within enclosures. Figure 16 shows the process flow diagram for the plant with the automated control loops used to ensure product quality. The number of unit operations is reduced from 21 for the batch process to 14 for the continuous process mainly due to improvements in the downstream steps using continuous flow technologies. For instance, steps such as mixing, granulation, drying, and compression forming are replaced by a single, integrated extrusion molding device. The process residence time is nominally 48 h which is nearly an order of magnitude shorter than the sum of the processing times for the batch process (300 h not including off-line holding and transport).[86] This is from realizing shorter processing time across all the unit operations (Table 1).

Scheme 1. Synthetic steps from intermediate, **1**, to aliskiren hemifumerate, **6**

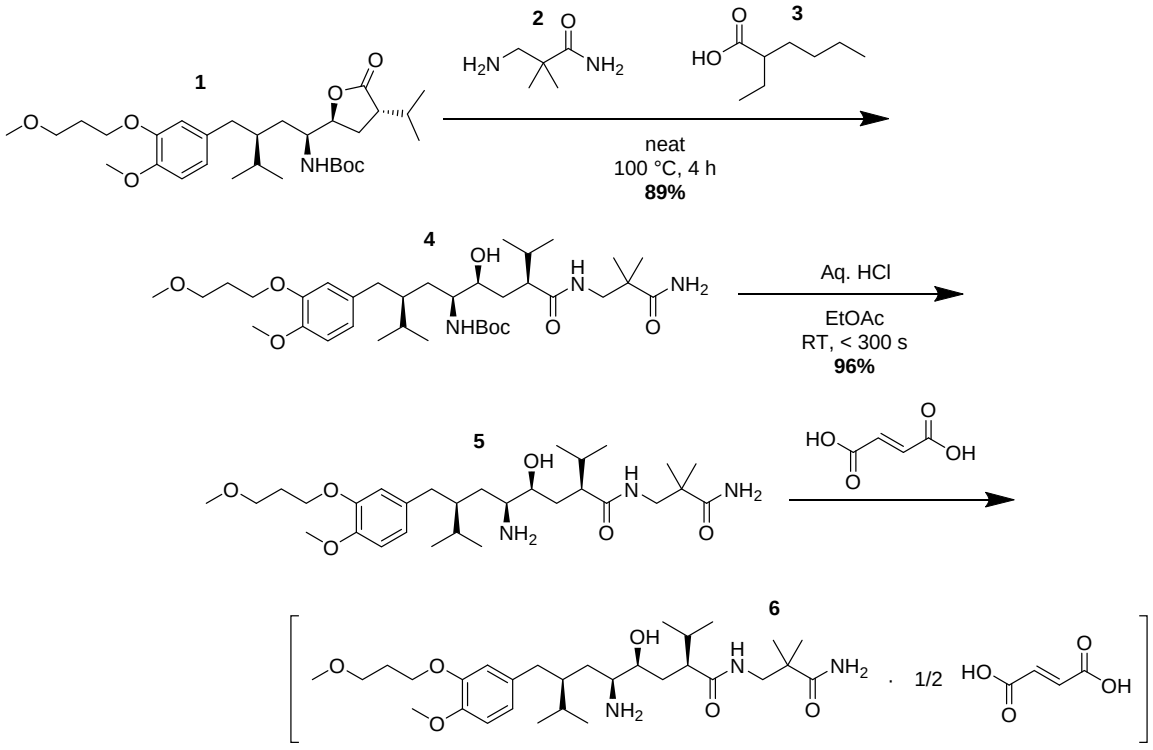

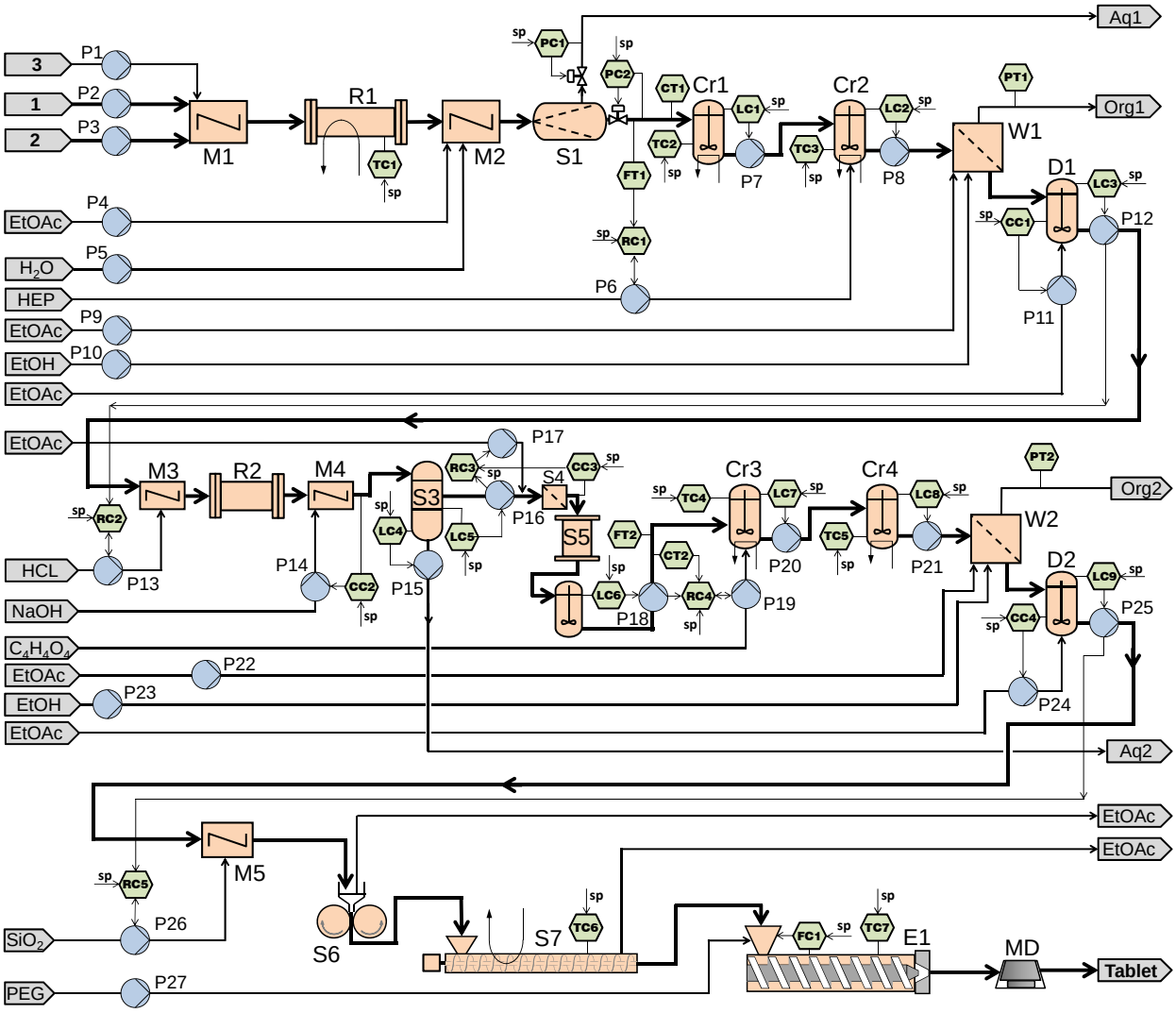

Figure 16. Process flow diagram with control loops. P – pump; M – mixer; R – reactor; TC – temperature controller; PC – pressure controller; CT – concentration transmitter; FT – flow transmitter; RC – ratio controller; S – separation; Cr – crystallization vessel; LC – level controller; PT – pressure transmitter; W – filter/wash; D – dilution tank; CC – concentration controller; FC – flow controller; E – extruder; MD – mold; sp – set point.

Table 4. Nominal residence times for continuous process

Unit operation[a]	*t* / min
R1	240
S1	1
Cr1+Cr2	480
W1	1
D1	120
R2	< 5
S3	120
S5	900
Cr3+Cr4	480
W2	1
D2	120
S6+S7	360
E1	10
MD	1

[a]Unit operations refer to designations given in Figure 16.

3.2.1 Upstream continuous synthesis and workup

While a detailed description of the process is provided in Appendix A, a brief description is provided here to highlight instances of advantages from the continuous and integrated features of the plant. The process starts with the chemical intermediate **1** that is melted and pumped into a tubular reactor (R1) at 100 °C where it combines with 10 equivalents of amine **2** and 1 equivalent of acid **3** and reacts reversibly to **4**. This reaction was developed[87] specifically for the flow process and provides several advantages over the batch process. Running neat in a single-phase reaction, the reaction is much faster than existing batch processes which can also produce solids (3–4 h vs. 72 h).[88-91] Workup is performed inline (M2) by adding water and ethyl acetate under pressure (7.5×10^5 Pa) at the reaction temperature to solubilize the reagents before cooling. This is more easily done in flow where the solvents are mixed at temperatures above their boiling points whereas in batch, cooling of the reaction crude results in a highly viscous liquid that is difficult to mix. The two-phase stream is separated using a membrane-based liquid-liquid separator (S1) that is scaled up from microfluidic flow applications.[14] The organic phase contains only **1** and **4** while the aqueous phase removes **2** and **3**.

The separated organic phase is fed into a two-stage, mixed suspension, mixed product removal (MSMPR) crystallization process (Cr1 and Cr2).[92] The solution is cooled to 5 °C and mixed with the antisolvent heptane. The slurry is then fed into an in-house built continuous filter

(W1). A thin layer of slurry is formed over a rotating, porous plate and is washed with ethyl acetate and ethanol. Vacuum applied to the back side of the plate pulls the mother liquor and wash solvent through and the purified wet cake is scraped off and conveyed into another vessel (D1). A density flow cell (CC1) in a side loop monitors the concentration of **4** in the vessel and feedback control adjusts the flow rate of an ethyl acetate dilution stream to adjust the concentration to 26.2 wt% as measured by the density meter required for the second reaction of **4** to **5** (shown in Scheme 1).

This movement of material from the crystallization through the filter into the second reaction provides an example where a critical material attribute (CMA) of a key intermediate is controlled within the process (Figure 17). Control for the process is split up into two layers: stabilizing and quality.[93] The stabilizing control layer consists of automated level control loops that maintain sufficient holdup in each vessel while the quality control layer maintains a desired product quality (by targeting CMAs). Figure 17 shows the propagation of a disturbance originating from Cr1 after several days of operation. The inlet flow rate to Cr2 dropped after the vessel had already been operating close to steady state. The stabilizing control layer includes level control for Cr2 and for D1 (Figure 17a–d). The controlled variable close to the disturbance, the level of Cr2, was not tightly controlled which absorbs the effects of the disturbance in throughput locally, decreasing the volume in Cr2 (Figure 17a), while mitigating effects downstream. The concentration of **4** going into the second reaction (R2) is a key intermediate CMA and is adjusted in the quality control layer. The solvent flow rate going into D1 follows the throughput disturbances passing through W1 more aggressively and reaches a minimum slightly after the outlet flow rate of Cr2 reaches a minimum (Figure 17b and f). As a result, the concentration of **4** in D1 does not show large variations (Figure 17e) which ensures a minimal effect of the disturbance on the performance of R2.

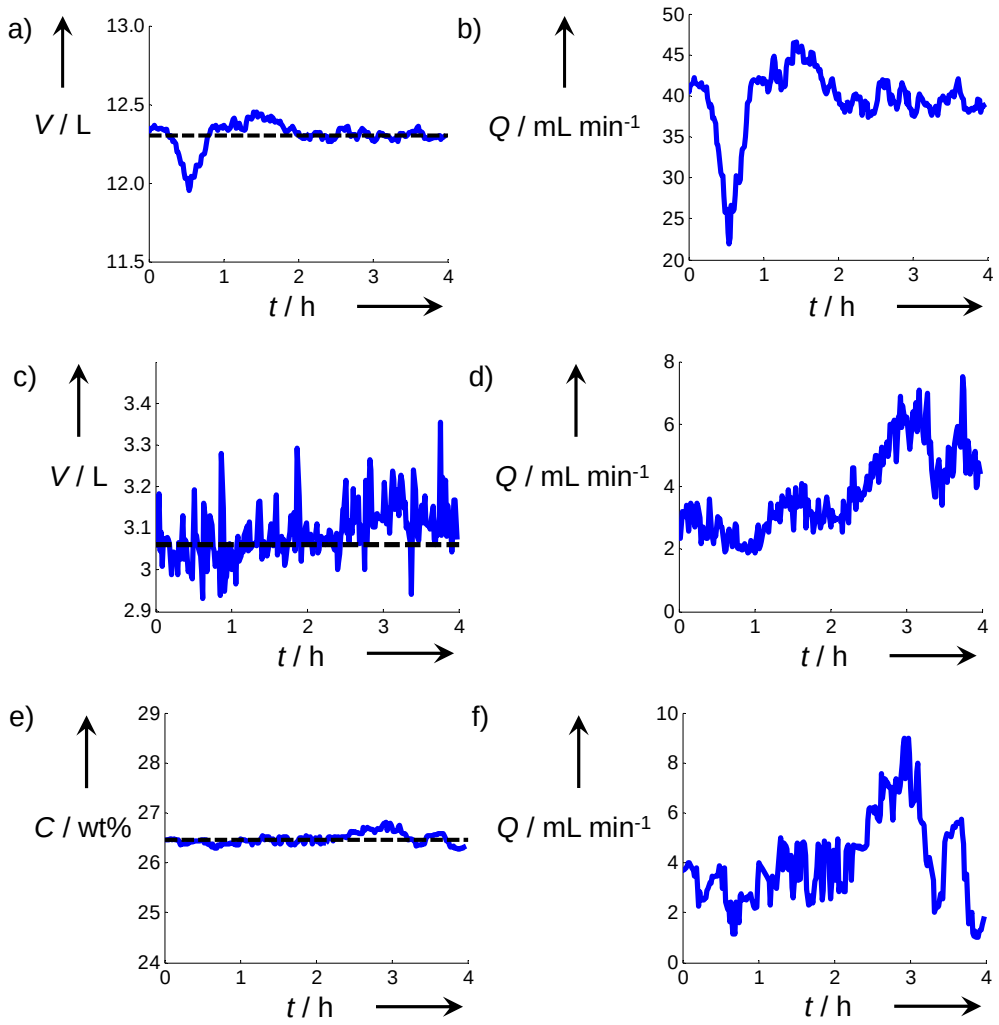

Figure 17. Example of disturbance mitigation through a cascade of three integrated unit operations after several days of operation, a) volume in Cr2, b) outlet flow rate of Cr 2, c) volume in D1, d) outlet flow rate of D1, e) concentration of **4** in D1, f) solvent flow rate into D1. The setpoints in a, c, and e are marked as horizontal dashed lines and a constant steady-state offset as a result of proportional-only control has been subtracted.

The second reaction is an acid-catalyzed removal of the Boc protecting group. This is done in a tubular reactor (R2) where concentrated HCl is mixed with the slurry of **4** in ethyl acetate. Control of the concentration of **4** is necessary to maintain the appropriate equivalents of acid in the reactor (16 equivalents HCl:**4**). Mixing is ensured by CO_2 formation in the reactor. The reaction is rapidly quenched on-line with 25 wt% NaOH which would produce a large exotherm if performed in batch. Under continuous flow, the temperature exiting the quench

remains around 40 °C without any cooling beyond convection from air circulation in the enclosure over the 1.6 mm ID × 3.2 mm OD × 2.5 m length PFA tubing that connected the reactor to the settling tank for liquid-liquid separation (S3).

Workup of the organic phase containing **5** requires a few steps that arise from operating the process continuously. The objective of the steps is to produce a stream with 6 wt% **5** in ethyl acetate with less than 0.1 wt% water starting with the 25 wt% **5** in ethyl acetate that has approximately 6 wt% water after contacting the aqueous quench stream.[94] The stream is continuously diluted with ethyl acetate which causes NaCl (from the quench) to precipitate. Microfiltration membranes (S4) remove the solid in order to clarify the solution prior to measuring the concentration with an inline UV flow cell used to control the dilution stream. Lastly, the stream is passed through a packed column (S5) of molecular sieves to remove water. The extra steps allow us to use a main solvent (ethyl acetate) through the whole process and avoid isolations and solvent swaps which would disrupt the flow of material through the process and require more challenging solids-handling processes.

A reactive crystallization[94] is performed to create and purify the final salt form (**6**). Fumaric acid is added using feed-forward control based on a second inline UV detector at a slight excess (0.55 acid:**5**). The material initially forms the salt in the first MSMPR vessel (Cr3) at 20 °C and then the yield is further increased by cooling in a second MSMPR vessel at −10 °C. The material is filtered and washed on a second continuous filter (W2) similar to W1. The wet cake is diluted to 15 wt% with ethyl acetate using feedback control from a density flow cell. Before drying the crystals for formulation, the first excipient (SiO_2) is added. The final crystals are needle-shaped (Figure 18) and flow poorly resulting in inconsistent tablet composition from fluctuations in the gravimetric powder feeder. Poor flowability is often solved by adding a glidant,[95] in our case 2.5 wt% SiO_2 on a dry basis. This is typically done late in the formulation process, however, that would require metering SiO_2 at 1.15 g h^{-1} which is well outside the capabilities of commercial powder feeders. This is solved by metering the SiO_2 in a slurry prior to drying. This would not be as easy to integrate if the traditionally upstream and downstream processes were disconnected and done in separate locations.

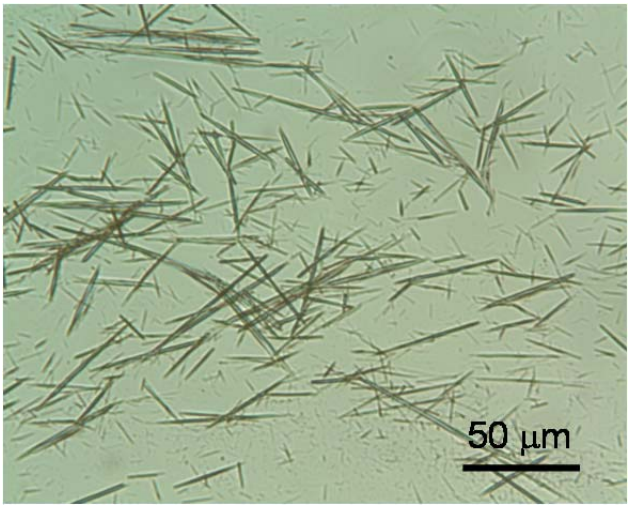

Figure 18. Micrograph of **6** crystals formed in Cr2.

3.2.2 Downstream formulation and tablet formation

The drying process (S6 and S7) also uses in-house built equipment. It involves two stages, the first dries the stream to less than 5 wt% solvent using two convection-heated drums that turn to produce a thin sheet of powder. The sheet is scraped off and broken into flakes that fall into a vacuum chamber that is periodically pumped down and opened to the vacuum drying stage. This consists of three 6 cm ID × 1.5 m long tubes with a rotating screw that conveys the powder. The tubes are heated at increasing temperatures (40, 60, and 75 °C) to prevent trapping of solvent inside the flakes due to rapid heating of the outside surfaces. The material exiting the dryer had less than 5,000 ppm of ethyl acetate (Figure 19). The dried powder is loaded into a gravimetric feeder using a vacuum conveyor alongside a second feeder with 6,000 Da polyethylene glycol (PEG). The two powders are metered at a mass ratio of 35:65 **6**:PEG into a twin screw extruder that continuously melts and mixes the materials at 60 °C.[96, 97] A tablet mold is coupled to the extruder outlet and forms the mixed material into tablets with a defined geometry which are ejected six at a time.

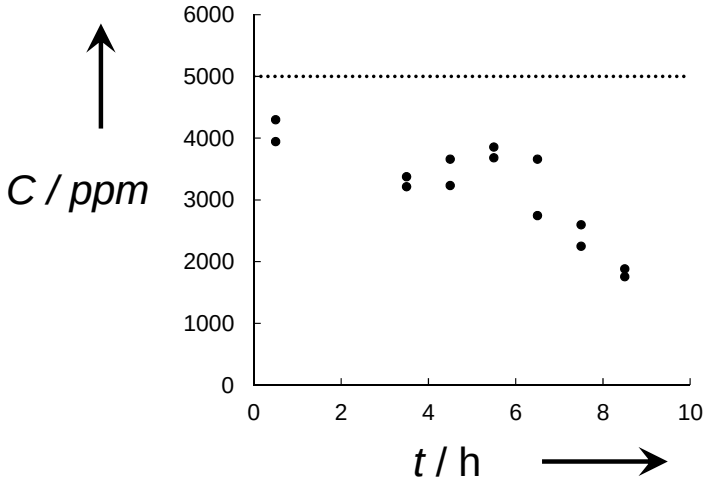

Figure 19. Plot of ethyl acetate content in dried **6** exiting the dryer (S7) with specification limit shown by a dotted line.

3.2.3 Final tablet quality

Finished tablets pass several tests of product quality. The tablets have a uniform visual appearance (Figure 22a) and have comparable size and dosage as commercial tablets. The tablets dissolve rapidly, faster than commercial tablets made of a different excipient (Figure 20), which puts them within specification for immediate release doses.[98] Residual solvents are also within specification[99] since no solvent is added after drying such as for granulation which is commonly performed in batch processing. The API retains characteristic crystalline peaks by x-ray diffraction in the final product after drying and processing through the extruder and mold (Figure 21). The tablets also pass content uniformity tests (Figure 22b and Appendix B).[100] The product contains only one significant impurity, **7**, which was kept to within specification[101] (Figure 22b).

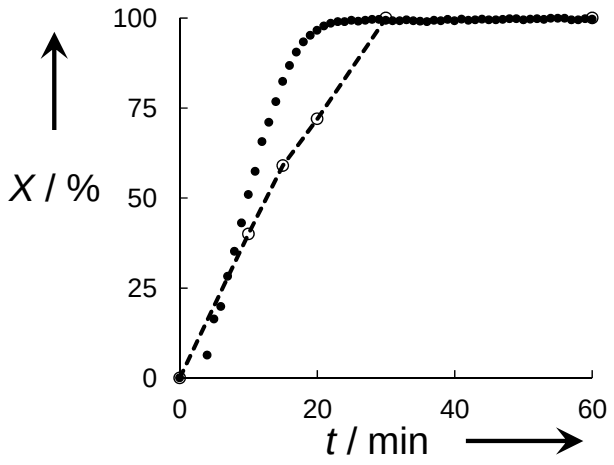

Figure 20. Dissolution profile (X, % dissolved) of dip coated tablet (filled circles) compared with commercial tablet (dashed line with open circles).

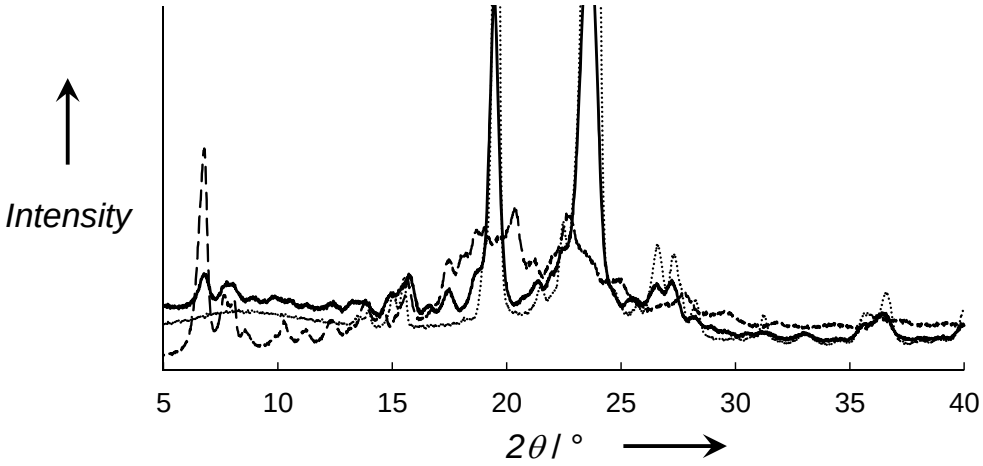

Figure 21. XRD patterns of PEG (dotted line), **6** following crystallization, filtration, and washing (dashed line), and formed tablet (solid line).

Scheme 2. Degradation pathways to the main impurity, **7**, present in the final product.

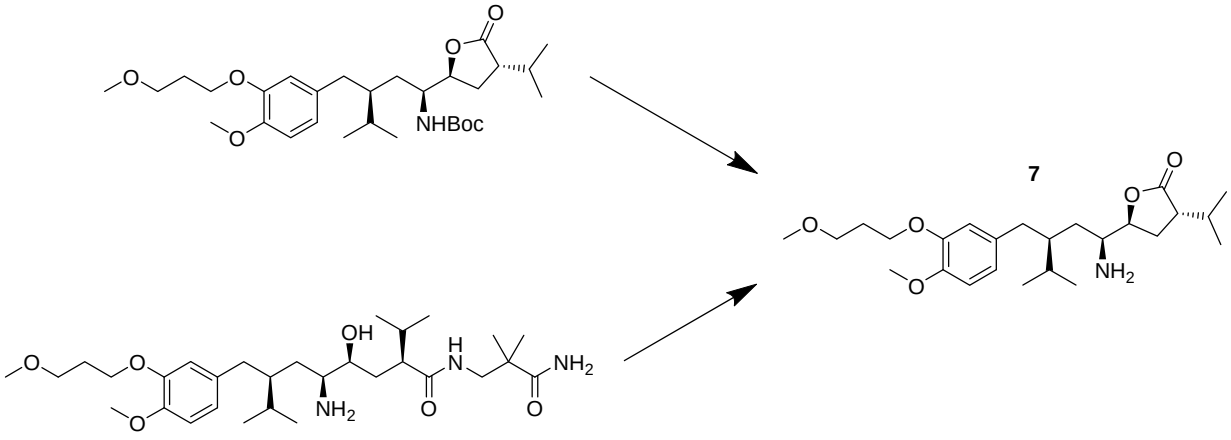

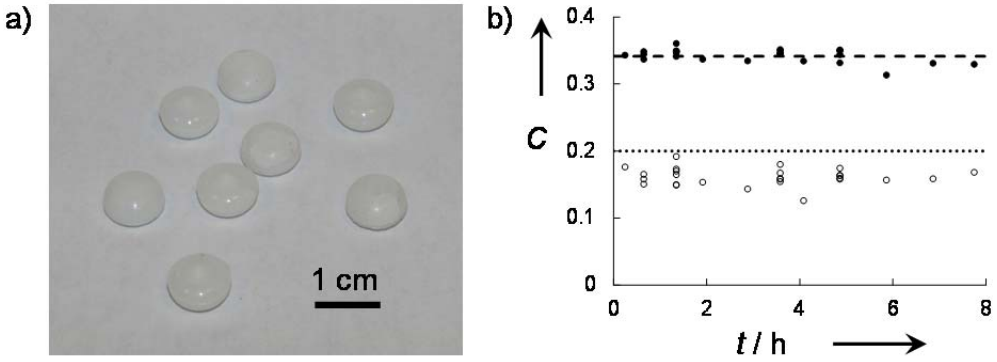

Figure 22. Analysis of tablets produced by integrated, continuous plant, a) photograph of uncoated tablets, b) tablet mass fraction of **6** (filled circles) with the nominal concentration shown with a dashed line (0.341) and % content of **7** (open circles) with specification limit shown with a dotted line (0.2 %).

The source of **7** present in the product can be traced back to several places in the process (Table 5) as both **1** and **5** can react to form it. The first is unreacted **1** that carries into the second reaction where it undergoes removal of the Boc group similar to **4**. The second is the reversible cyclization to reform the lactone from **5** which can occur spontaneously at higher temperatures. The conditions in R1 are optimized to increase the conversion of **1** to limit the amount of **1** entering the first crystallization and filtration. The crystallizations and filtration/washings are optimized to minimize the amount of impurities carried into subsequent steps from temporary impurity spikes by using excess washing solvent. The three temperature zones in the vacuum

dryer expose the API to high temperatures for a shorter time once the majority of the solvent is removed. Use of PEG in the extrusion and molding reduces the temperature required to the melting point of PEG (Figure 23), rather than operating as a melt extrusion at the melting point of the API.

Table 5. Levels of key impurities throughout process. Values of area% are based on peak area from HPLC. This value is close to the mol% given similar chromophore and high purity of most streams.

Process position	*C* / area% product	*C* / area% impurity
S1 to Cr1[a]	89.5	4.8
D1 to M3[a]	98.7	0.18
M4 to S3[b]	93.0	2.3
D2 to M5[c]	99.5	0.10
S7 to E1[c]	99.7	0.11
Final tablet[c]	99.7	0.13

[a]Product is **4** and impurity is **1** which is not observed downstream of R2.
[b]Product is **5** and impurity is **7**.
[c]Product is **6** and impurity is **7**.

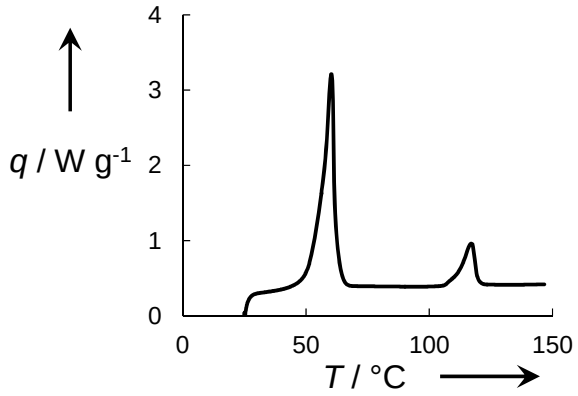

Figure 23. Differential scanning calorimetry of interior of a PEG coated tablet showing PEG melting point at 60 °C and **6** melting point at 117 °C. Arrow shows direction of endothermic heat flow.

Lastly, an in-house built continuous, solvent-free dip-coating process was tested during portions of the continuous runs to observe the effect on product stability. While the tablets produced met impurity level requirements when tested immediately, the tablets would fail when subjected to accelerated ageing conditions in stability chambers (Figure 24). The PEG coating

was not completely uniform (Figure 25) but it coated tablets showed reduced amounts of **7**. This may be due to lower water content in the dip coated tablets (0.65 wt% in dip coated compared to 0.92 wt% in the uncoated tablets prior to placement in the humidity chamber). It is known that the tablets are sensitive to moisture and are therefore stored with a desiccant.[96] Additional improvements to the coating process should further increase product stability as some tablets had thin or incomplete coating. Additionally, there were very few dip coated tablets produced so there were not enough samples to take duplicates at each time point. More data points would improve the quality of the trends to better observe any difference coating tablets makes.

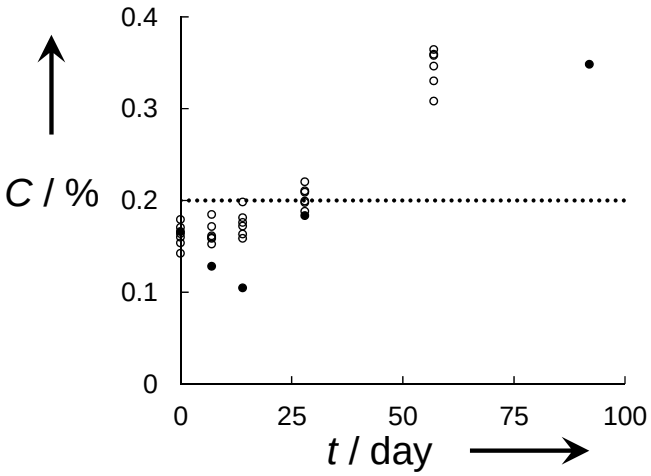

Figure 24. Accelerated stability test results for % content **7** for uncoated (open circles) and dip coated (filled circles) tablets with 0.2 % specification limit shown as a dotted line.

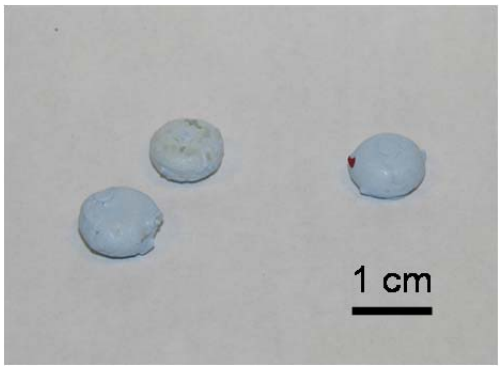

Figure 25. Photograph of continuously dip coat tablets. Note that the red coloring is due to contact with separate, red colored coated material from previous tests.

3.3 Conclusions

In summary, a continuous pharmaceutical plant that integrates chemical synthesis, purification, formulation, and tableting was developed and operated. From chemical synthesis to tableting, the entire process runs continuously. An automated control system monitors and controls the process to maintain product quality. Several new pieces of continuous equipment are used. The process is redesigned changing many aspects of the batch process to avoid issues with solids handling and eliminating solvent swaps. The final tablets meet specifications for drug product quality. Future work in this area will involve developing and understanding new continuous processes and show their application across a range of drug products. This will be done alongside collaborations with industry and regulators to aid in translating these innovations beyond the lab.

Chapter 4. Performance of the synthesis and workup steps in the continuous plant

4.1 Introduction

This chapter continues the results presented on the continuous pilot plant in Chapter 3. Specifically, the two synthetic steps and corresponding workup will be examined from development through operation. The pilot plant provides a concrete example to study continuous processing and the various aspects of it.

A unique aspect of the pharmaceutical industry is the drive for processes operating at multiple production scales. Although microreactors are used for early flow chemistry development and many commodity chemical processes are performed at large scale in flow, there is much less work done at an intermediate production scale. This is a relevant scale for the pharmaceutical industry where production at the hundreds of grams to kilogram scale is necessary during development, particularly for preclinical and clinical trials, prior to full scale, commercial production. There is a distinct lack of research and availability of equipment at this scale. Additionally, while many single reaction steps have been demonstrated, relatively few integrated processes have been documented incorporating multiple reactions or reactions with workups relevant to pharmaceutical processes.[15, 16, 20, 27, 37, 68, 69, 102] Developing a fully integrated process (defined as operating all reaction and purification steps linked together and run without isolation and offline holding) requires global optimization of unit operations across the whole process resulting in conditions that may not be optimal for any single step.[64]

This chapter highlights how a specifically tailored batch process (designed to be amenable to flow) can be translated into flow with the use of residence time distribution models. Some solutions to common issues in translating flow processes are presented in the context of the synthesis of aliskiren, **5**. Lastly, the benefits of flow used in the process are emphasized.

4.2 Results and discussion

4.2.1 First reaction and workup steps

The process starts with the reaction of lactone **1** and amine **2** to form the amide intermediate **4** (Scheme 1). The reaction runs solvent-free in a molten condition and was previously reported in a batch system with the objective to develop conditions amenable to flow.[87] This transformation was significantly improved over previous conditions with long reaction times (72 h), lower yields, and handling of insoluble slurries at lower temperatures.[88-91] The yields were further optimized in batch by decreasing the reaction temperature and increasing the equivalents of **2** (Table 6). A longer reaction time is required due to the slower reaction rate at the lower temperature. Temperatures lower than 100 °C are not practical as the melt becomes difficult to stir due to high viscosity. It is worth noting that more than 10 equivalents of **2** results in lower yields despite the higher equivalents, which is likely due to dilution of the reaction. Therefore, 100 °C, 10 equivalents of **2**, and 1 equivalent of **3** is used in the process to maximize yield while maintaining short reaction times and avoiding solid formation.

Table 6. Reaction condition screening for conversion of **1** to **4**[a]

Time / h	Temperature / °C	Equivalents **2**	Conversion **1**[b]	Yield **4**[b]
1	120	5	0.86	0.80
3	100	5	0.92	0.87
3	100	10	0.95	0.89
3	100	15	0.95	0.89
3	100	20	0.94	0.87

[a]All conditions run with 1 equivalent of **4** in batch.

[b]Fraction based on HPLC area.[103]

Figure 26 shows the dynamic development of the yield of **4** during a batch reaction for higher and lower temperature conditions selected from Table 6. After a rapid rise to a maximum yield, a slow degradation takes place and reduces the yield at both temperatures. However, the degradation rate is less dramatic for the lower temperature, which makes the reaction less sensitive to changes in the reaction time beyond the time to reach equilibrium. Differences in reaction times can arise in flow due to the residence time distribution created by flow reactors.

Fluctuations in flow rate related to throughput changes can also directly affect the reaction time. The lower reaction temperature conditions are used as it makes the yield less sensitive to disturbances.

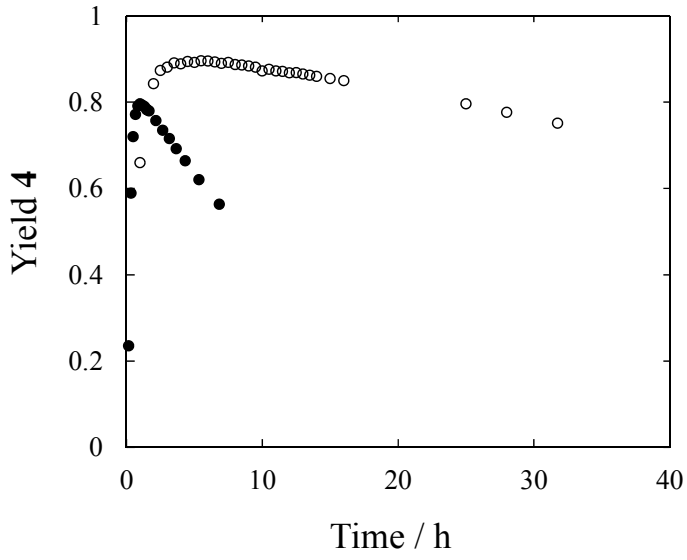

Figure 26. Batch reaction performance over time at 120 °C with 5 equivalents **2** (solid circles) and 100 °C with 10 equivalents **2** (open circles). Both reactions use 1 equivalent of **3** and the yield fraction is measured by HPLC area.

A simple tube reactor is used as the reaction is relatively slow and not affected by mass or heat transfer limitations. While initially the reagents are rapidly mixed with a static mixer, the flow through the tube will undergo residence time broadening due to convection and dispersion. The reactor is sized such that these effects do not adversely affect the yield. This is done by combining the time course data in Figure 26 with models of the residence time distribution.[104] Since the system is initially well mixed, the yield can be determined by taking the convolution integral of the time evolution of the yield and residence time distribution:

$$\overline{Y} = \int_0^\infty Y(t) \cdot E(t)\, dt \tag{12}$$

where $\overline{Y}$ is the average yield exiting the reactor; $Y(t)$ is the yield as a function of reaction time, t; and $E(t)$ is the residence time distribution. The values of $Y(t)$ were measured experimentally in a batch reactor (Figure 26) and $E(t)$ can be predicted from models depending on the flow pattern in

the reactor. A relatively large tube ID (1.17 cm) is selected to limit the length required (25 m for the final design) so the reactor would fit within an oven used to maintain the reaction temperature (100 °C). Using a nominal total flow rate of 675 mL h^{-1} (to meet the target throughput of the entire process) and a diffusion coefficient of 1×10^{-9} m^2 s^{-1} (typical value for small, organic molecules), results in conditions where the reactor performance is predicted to lie between the convection model where only the laminar flow profile is considered and the dispersion model which includes diffusion across streamlines.[105] Both models are tested since there is uncertainty in the exact diffusion coefficient (due to solvent-free conditions and high viscosity). This provides a range for the reactor performance between the convection model and the dispersion model. The reactor yield is estimated by numerically integrating Equation (12) with the results summarized in Table 7. From these results, a reactor with a nominal residence time of 4 h is selected as the model predictions were not sensitive to the difference between the convection and dispersion models and yield is not predicted to be significantly higher for longer residence times.

Table 7. Estimated reactor performance for conversion of **1** to **4** (Scheme 1) accounting for residence time distribution in flow

Residence time / h	Batch result		Convection model		Dispersion model	
	Conversion **2**	Yield **5**	Conversion **2**	Yield **5**	Conversion **2**	Yield **5**
3	0.95	0.88	0.90	0.84	0.94	0.88
4	0.96	0.89	0.94	0.87	0.96	0.89
5	0.96	0.89	0.95	0.88	0.96	0.89

The final process configuration is outlined in Figure 27. The crude product leaving the reactor is dissolved in water and ethyl acetate while still heated to prevent solidification if the crude melt is cooled. A pressure controller operating at 7 bar prevents the solvents from boiling when heated prior to mixing. The reactor performance over the course of the run is similar to that predicted by the model (Figure 28a). Samples are taken of the organic phase following liquid-liquid separation. The concentration of **4** in the aqueous phase is less than 1 % of the concentration in the organic phase with similar volumes of each phase produced. No **1** is detected in the aqueous phase. This process makes use of a simple workup procedure where a

single extraction stage recovered nearly all **4** at high concentration (13 wt% **4**, nearly saturated in **4**, Figure 28b). The high concentration is used to increase the yield in the subsequent crystallization step.

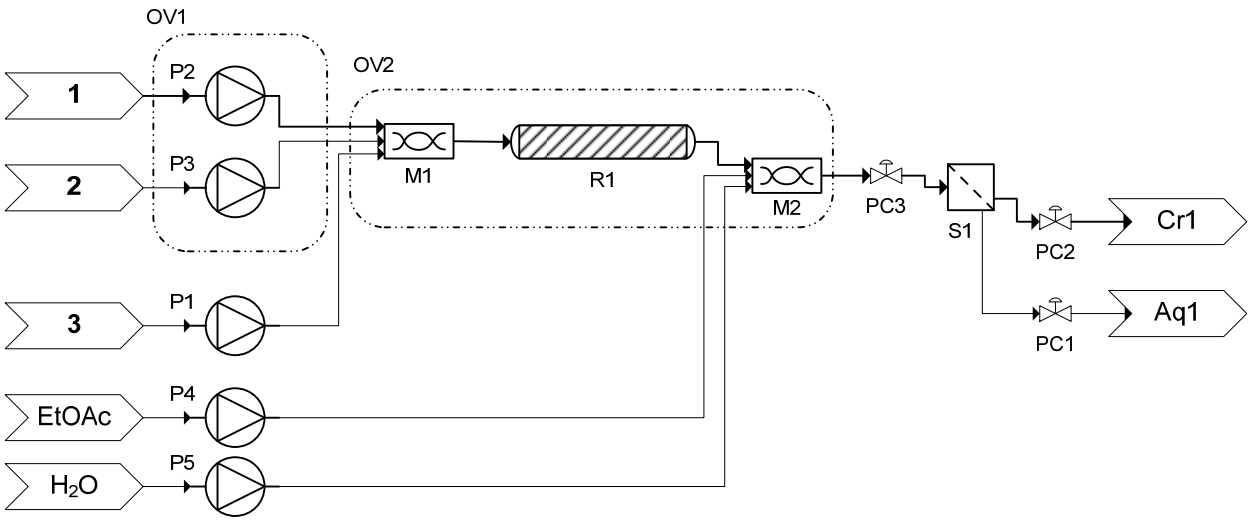

Figure 27. Process flow diagram for synthesis and workup of **4**. OV – oven; P – pump; M – mixer; R – reactor; PC – pressure controller; S – liquid-liquid separator; Aq – aqueous waste; Cr – crystallizer.

Liquid-liquid separation is performed using twelve scaled-up, membrane-based separators (Design 4, Figure 15d).[14] Operating membrane-based separators requires careful control of pressure balanced against the interfacial tension, Equation (1).[14, 16, 46, 47] The contact angle with polytetrafluoroethylene (PTFE) for most aqueous-organic systems is high (160° in this case) so the dominant system parameter for designing the separator (pore and channel dimensions) is the interfacial tension. The interfacial tension for this system is only 1.7×10^{-3} N m^{-1} which is much lower than most systems, including water-ethyl acetate at 6.8×10^{-3} N m^{-1}. Using 1 μm pore size membranes (to limit pressure drop for flow through the membrane), this corresponds to a Laplace pressure of 6.4×10^{3} Pa. The pressure is therefore carefully controlled by two backpressure regulators located on the aqueous and organic outlets. Some loss of organic phase to the aqueous outlet is allowed to ensure that the organic stream passing through the membrane is not contaminated with any aqueous phase (Figure 28b). The membrane performance was steady for approximately 100 h after which there was a slow increase in

retention of organic phase likely due to fouling of the membranes. The controlled pressure was not adjusted as the downstream processes were operating in closed-loop mode and adjusted automatically to changes in throughput. Performance could be maintained by additional separators that could be brought online when fouling occurs while fouled membranes are cleaned or replaced. Following liquid-liquid separation, the organic phase is fed into two continuous crystallizers[92] and is then filtered and washed continuously. The resulting stream is 98.7 % pure by HPLC.

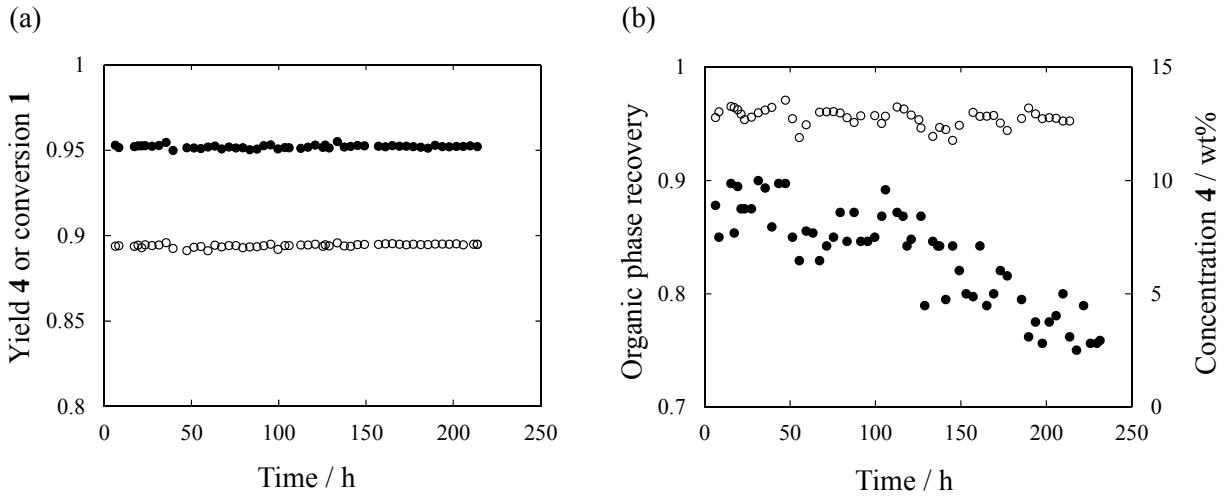

Figure 28. (a) Continuous reactor performance for conversion of **1** to **4**. Filled circles are fraction conversion of **1**. Open circles are fraction yield of **4**. Values from HPLC area. (b) Continuous liquid-liquid extraction and separation performance. Filled circles are fraction of organic phase recovered. Open circles are concentration of **4** in the organic phase.

4.2.2 Second reaction and workup steps

The second reaction removes the Boc group from **4** to form **5**. This is done by treating a slurry of **4** in ethyl acetate with an excess of concentrated aqueous HCl. HCl is selected over other deprotection agents because of its low cost and simple, high concentration workup by addition of NaOH to form NaCl (a basic, high ionic strength aqueous phase to increase recovery of **5**). The reaction conditions were optimized by testing in flow. The reaction forms CO_2 that creates irregular flow patterns in larger tubes (ID = 0.40 cm) due to the liquid phase settling in the bottom of the coiled tube. The coil is oriented with the axis of the coil parallel the ground.

The movement of the gas does appear to improve mixing in the reactor by streaming through the liquid in the vertical portions of the coiled tube. The reaction is run at half scale and the reactor duplicated in the plant by feeding with peristaltic pumps equipped with two heads to support two parallel flow lines at the same flow rate. Figure 29 shows the performance of a 4.9 m long reactor. The reactor is operated at 30 °C because higher temperatures result in increased degradation. A slurry concentration of approximately 25 wt% is selected to obtain high yields while avoiding frequent clogging. Slurry concentrations greater than 30 wt% **5** are difficult to pump and were found to frequently clog the lines used to convey the slurry to the reactor. A value of 16 equivalents of HCl:**5** is selected since higher equivalents increased degradation. Also, using greater than 12 equivalents of HCl results in low sensitivity of the reactor performance to throughput changes. This is important as the level control loops on the process vessels introduce fluctuations into the flow rate of the **4** slurry entering the reactor.

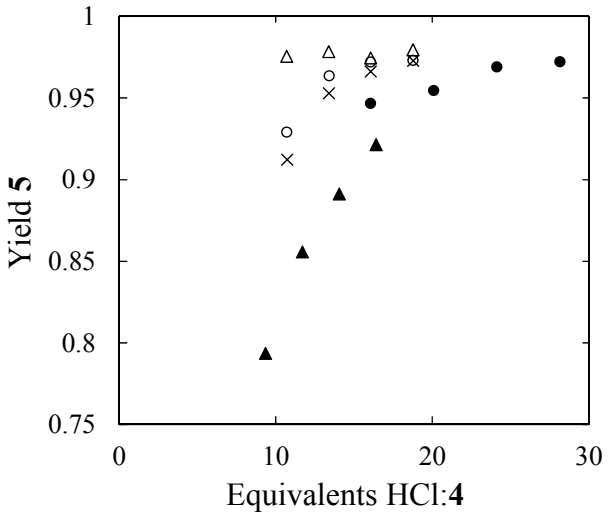

Figure 29. Continuous reactor performance for conversion of **4** to **5** operating at 30 °C. Filled circles: 353 mL h^{-1} of 20 wt% **4**; filled triangles: 605 mL h^{-1} of 20 wt% **4**; open circles 219 mL h^{-1} of 30 wt% **4**; open triangles 278 mL h^{-1} of 30 wt% **4**; crosses 333 mL h^{-1} of 30 wt% **4**. Yield given as fraction based on HPLC area.

Increasing the reaction time creates additional side products so the reaction is rapidly halted by inline quenching with 25 wt% aqueous NaOH. While this is an extremely exothermic reaction, the temperature rise in the fluid exiting the reactor is only about 10 °C by the time the

stream reached the next unit operation, approximately 10 s through 1.6 mm ID × 3.2 mm OD perfluoroalkoxy (PFA) tubing. The limited amount of HCl quenched at any given time means the convection from air flow over the tubing in the enclosure is sufficient to control temperature. The quench was initially performed by combining the NaOH and crude product in a tee mixer; however, the tee would periodically clog with NaCl formed by the acid-base reaction. Under this configuration the reactor would only operate for 1-2 h before clogging at the quench. Small scale batch experiments show that when incompletely quenched, solid NaCl precipitates out of solution and goes back into solution as additional aqueous NaOH is added. The mixing is improved by using a PTFE static mixer and introducing the crude product stream in the center of the channel with the NaOH stream in the annulus around the crude (Figure 30). CO_2 formed from the previous reaction step also helps mix the two streams during neutralization. This reduces the chance that incompletely quenched material with solid NaCl reaches the wall by sheathing the product stream in a more dilute NaOH stream. The material exiting the static mixer segment contains no observable solids, and clogging at the outlet is eliminated. The final system design is shown in Figure 31.

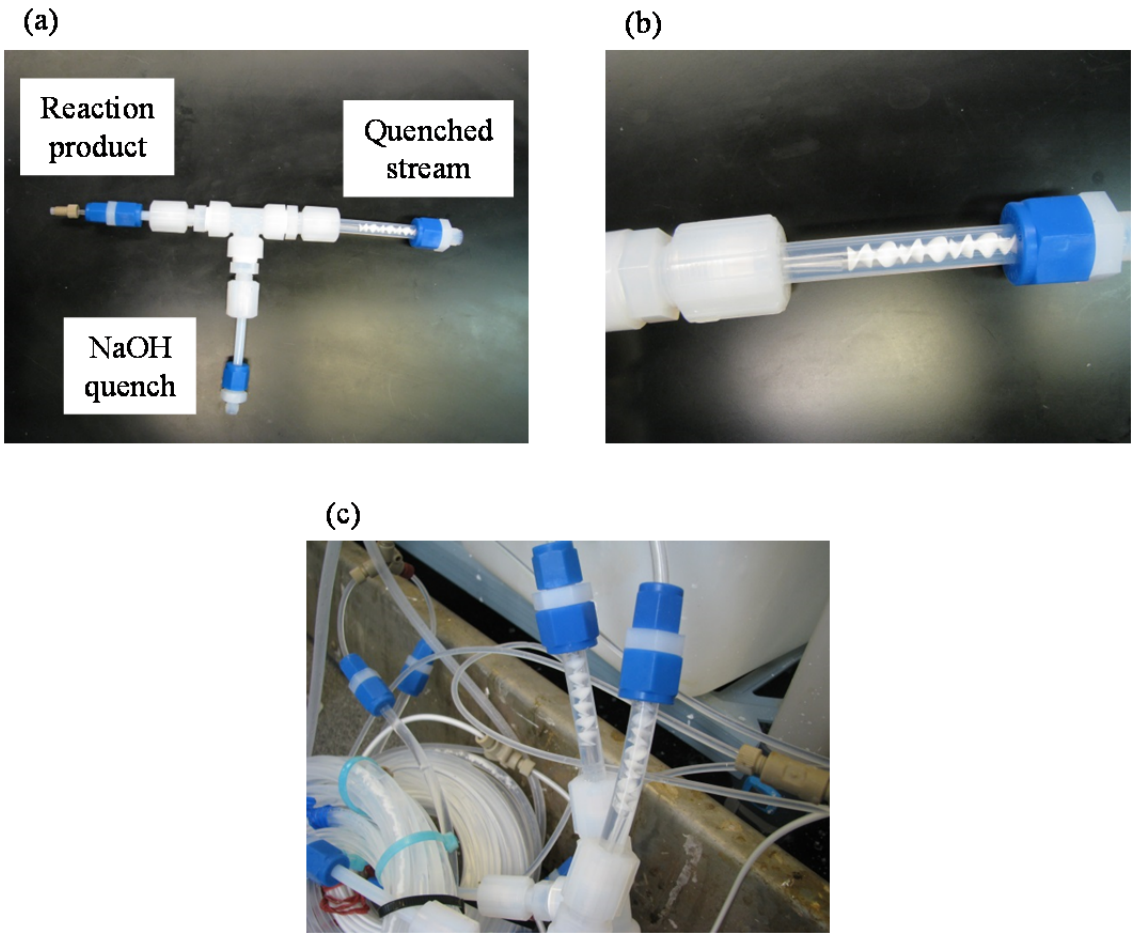

Figure 30. (a) Photograph of mixing section with tee inlets and mixer. (b) Detailed photograph of mixing section with tube-in-tube inlet and static mixer. (c) Quench mixer in use.

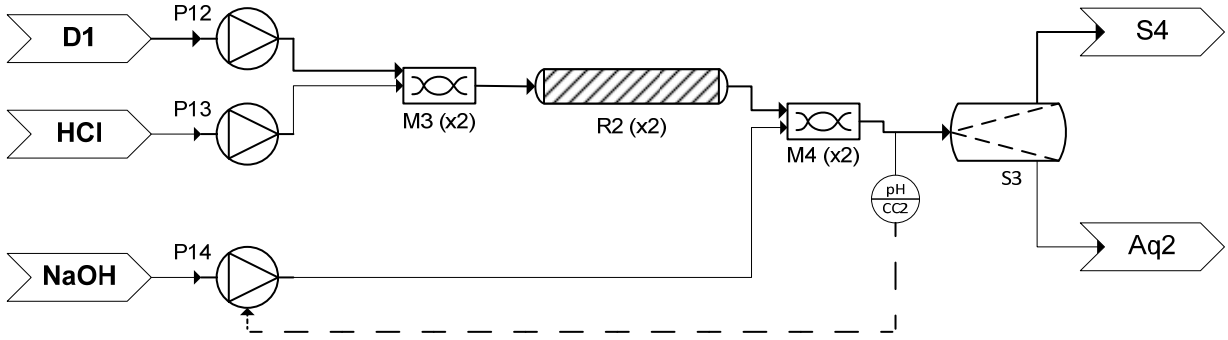

Figure 31. Process flow diagram for synthesis of **5** from **4**. P – pump; M – mixer; R – reactor; pH – pH probe; CC – concentration controller; S – separator; Aq – aqueous waste.

Figure 32 shows the performance of the deprotection reaction during the run. The yield performance (Figure 32a) is within the range observed for 16 equivalents of HCl during development (Figure 29). Fluctuations in the yield are due to fluctuations in the reactor from the inlet flow rate (Figure 32b) and clogs on the inlet from portions of slurry with high **4** concentration. One clogging event is shown in Figure 32b at 124 h where one of the feed lines to the reactor was clogged and quickly cleared. A temporary dip in pH is observed when the flow rate of the slurry increases to compensate for the increased level in the tank containing the slurry. The automated control quickly brings the pH back to the setpoint, 12, and maintains the pH even with the high level of fluctuations observed in the slurry flow rate. The quenched stream forms a two-phase system with an aqueous NaCl phase and an organic ethyl acetate phase containing **5**. The settling tank, S3, provides some buffering capacity from back-mixing to absorb any small dips in pH or yield. The organic phase is then fed to a continuous, reactive crystallization[94] where the hemifumarate salt is formed. The solid is then filtered and washed resulting in a purified drug substance.

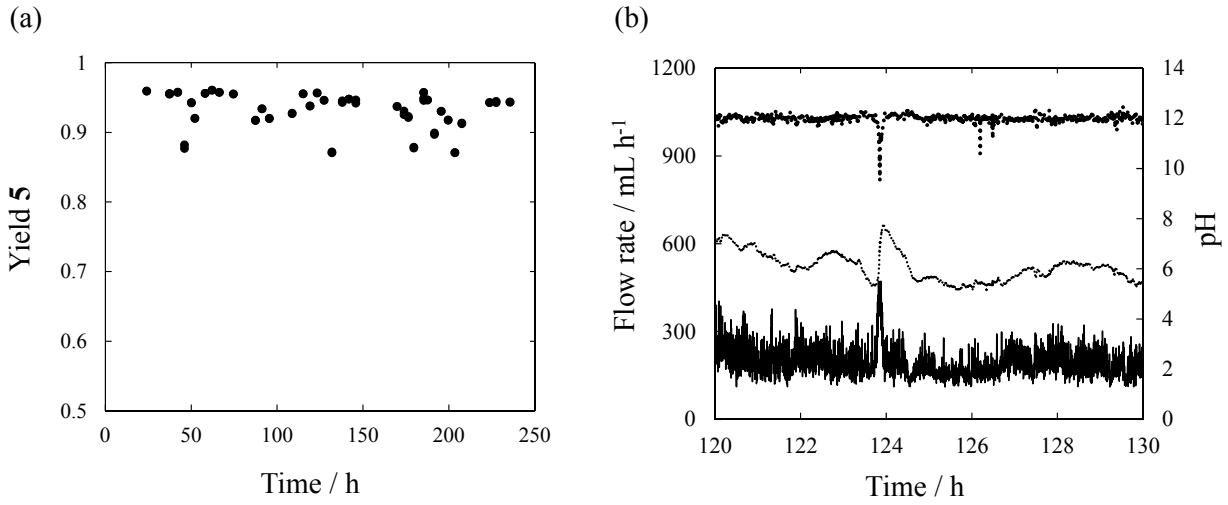

Figure 32. (a) Continuous reactor performance for conversion of **4** to **5**. Yield fraction based on HPLC area of organic phase samples collected after quenching before entering S3. (b) Continuous quench performance. Top dark dotted line is the pH; middle light dotted line is the flow rate of NaOH; bottom solid line is flow rate of **4** slurry. Flow rates are given as single reactor values (total is double the value for paired reactors). Data are collected every 10 s.

4.3 Conclusions

The results presented here detail the reaction and workup steps from the successful operation of a fully integrated, continuous manufacturing process for a pharmaceutical product. The design of the process required overcoming common problems related to flow, including solids handling and long reaction times. The first reaction (**1** to **4**) operates at 90 % yield, higher than previously reported conditions, and remains steady throughout the run. Workup of the crude reaction product is performed inline by liquid-liquid extraction and produced material that is continuously carried into a second Boc deprotection reaction. The second reaction (**4** to **5**) is run using automated control to reject disturbance from the process and maintains yields of 90-95 % even in the presence of disturbances. A rapid acid-base quench made use of the high heat transfer obtained in continuous flow to keep the exotherm low. The entire process was run for nearly 250 h at a nominal production rate of 41 g h^{-1} of aliskiren. The process could be improved to dynamically adjust pressures for the membrane separators and reduce instances of clogging due to slurry flow. This plant demonstrates the necessity of reevaluating the entire pharmaceutical manufacturing process with the intent to perform the synthesis in flow, as none of the steps are the same as the current batch process. However, this presents significant room for innovation as entirely new pathways can be developed using new processing steps available to continuous manufacturing.

Chapter 5. Conclusions and future work

5.1 Summary of thesis contributions

The main contributions of this thesis center on the development of scaled-up continuous chemical synthesis systems. Interest in the organic chemistry community regarding continuous flow processes in the past decade has focused mainly on microreactors. While microreactors provide a robust platform for flow chemistry and can take advantage of many features of flow chemistry, they are ultimately limited to screening reaction conditions and the smallest of production rates. The fine chemical and especially the pharmaceutical industries require larger scales, specifically the milliscale where 10-100 g per h of production is achieved. The creation of a fully integrated, continuous manufacturing process was adopted as a challenge to not only demonstrate the benefits of continuous manufacturing, but push the field forward by developing new technologies to fill gaps.

One particular gap that was addressed in this thesis was simple, small-scale liquid-liquid separators (Chapter 2). Membrane-based separators were previously developed for microscale processes where interfacial forces dominate over gravity forces. A larger scale separator would ease scale-up by keeping a similar unit operation from microscale to milliscale where a change to more conventional unit operations (such as settling tanks or centrifugation) at the same scale could be performed. The design and control parameters for the microscale system were based on flow resistance, but a closer examination of the relevant physics showed that pressure is the real parameter of importance. This understanding was initially used to create larger membrane separators. Eventually, an integrated pressure controller was added which guaranteed separation across a range of conditions. This greatly simplified operation of the separators by eliminating any external control. Additionally, the differential pressure controller allowed the simple creation of multistep separations where backpressure controllers, additional separators, or even pumps could be connected downstream of the separator. This feature was used to perform solvent swaps and countercurrent extraction processes.

The highlight of this thesis is the design and operation of a fully integrated continuous manufacturing plant for a pharmaceutical product (Chapter 3). The target product was tablets containing the small molecule drug aliskiren. The process was used as a test case to show that an

industrially relevant plant that was fully connected from synthesis through tablet formation was possible. The plant was built at a 45 g h^{-1} of drug substance scale which would be relevant for phase 3 clinical trials or even production of a low volume product. The entire process was operated continuously without breaks or isolations and was operated under closed-loop control to limit the manual intervention required. Both upstream synthesis and purification and downstream formulation and formation were integrated together. This required a close collaboration between the two sections in order to produce a final tablet that met performance criteria. Several new pieces of equipment were built and successfully tested within this process.

The reaction and workup steps were of particular interest (Chapter 4). Two reactions with the associated workup were translated from batch into flow. This required a complete change from the existing processes. Solids, a common source of problems in flow systems, were avoided by running the first reaction solvent-free at high temperatures. The reaction crude was then dissolved under pressure with a superheated solvent. This is a pathway that would be difficult to investigate and implement in batch. The subsequent liquid-liquid extraction workup provided a challenging system to test the membrane-based separators at high throughputs. The second reaction was run fast at high concentrations and was quickly quenched with an acid-base neutralization. This step made use of the higher heat transfer available in flow. The new process highlights a key learning that developing a flow process often requires completely redesigning the whole process rather than a more direct conversion from the batch process. All the steps in flow were substantially different from the batch process. The transformations were an improvement (faster, higher yields) over the existing process, but were inspired by specifically looking into flow processes.

5.2 Future work and outlook

The membrane separators provide a few future paths that appear quite promising. So far only a proof of concept countercurrent extraction with three stages was demonstrated. This required a pump for each stage. Since pumps are often the most expensive piece of equipment in a continuous process, this design for countercurrent extraction is not feasible for extending to challenging systems which can require > 10 stages. One way to get around this is to use a multi-head peristaltic pump which allows several streams to be operated off of one drive at the same flow rate. Since the pressure control diaphragm in the separator limits negative pressures

from being transmitted back through to the aqueous side, the pump can be attached to the aqueous outlet and operated at a high flow rate to convey the organic phase countercurrent to the organic phase (which can be moved by a single pump). This works because peristaltic pumps can draw against a dead ended tube and will not fail if pumping faster than the rate liquid exits the separator.

Another direction to take the scaled up separators is evaporation and eventually countercurrent distillation. It has already been shown that distillation can be performed using the microfiltration membrane to separate the gas and vapor phases.[50] Multistep processes, especially countercurrent distillation, would be affected by condensation of the vapor phase between each stage resulting in pressure disturbances that could affect upstream units. The same principle that allows a pump to operate on the aqueous outlet (see above) would also prevent the condensation of the vapor (which exits the retentate/aqueous outlet) from affecting the separation performance. There are still questions as to how the membrane and diaphragm will hold up at elevated temperatures which will require additional investigation.

Access to small scale, continuous evaporators would be valuable in many continuous processes, especially those involving a recycle stream. Recycling of the filtrate in a plant for recycling back to crystallization or reaction requires concentration of the diluted stream continuously by evaporation. Incorporating a recycle stream has been shown to have positive effects on process yield and other performance metrics for processes similar to the plant discussed in this thesis.[65] Within the existing regulatory framework, recycling is a procedure actually adapted to flow than batch. While in batch each cycle of the recycled material would need to be validated and tested to meet Good Manufacturing Practice, continuous processes eventually reach a steady state where the recycled stream is time invariant meaning further validation is unnecessary. This makes recycle a potential source of process improvement not currently easily available in batch, but readily enabled in flow.

One direction the plant was approaching, but never achieved, was acting as a demonstration unit for advanced control strategies, specifically model predictive control (MPC). In order to implement MPC, an accurate dynamic model of the process is required with accurate parameters fitted from process data. The process would need to be operated more to develop the models. However, once completed, having the end-to-end system available to test MPC would

show the immense power of MPC to take control actions to maintain the critical quality attributes within acceptable ranges by making changes throughout the process.

Throughout the time spent building the plant, many companies visited the lab to better understand what is being done with continuous manufacturing in the pharmaceutical industry. The same question was on all of their minds, "Will flow completely replace batch?" Based on the results obtained here, the answer is still no, but flow is not going away either. The fact that an entire process could be constructed at a relatively small scale (compared to production) provides support that a fully integrated system is possible for an industrially relevant product. It was found that starting early in the development process searching for flow amenable steps is critical as it is often very difficult to directly translate a process initially designed for batch.

One key insight into developing integrated continuous manufacturing processes is the importance of incorporating engineers early in the process to work with the chemist developing the synthetic route. The increased use of automated control and utilizing high heat and mass transfer are characteristic challenges encountered when developing a continuous process. The close collaboration between chemists and engineers is something increasingly seen within the pharmaceutical and fine chemical industry. Also required are more simple-to-use devices which can act as replacements for the widely available and highly flexible glass vessels typically used. Tube reactors with tee mixers are one example of a simple system which can be readily applied by researchers in many situations with little technical expertise required. The integrated pressure controller in the separator is another example of a device that mirrors the simplicity of the shake flask it replaces. It has a wide range of applicability and is simple to use, requiring minimal training beyond attaching the connections on the inlet and outlet. Overall, the field of continuous manufacturing is growing broader with a lower barrier to entry that will further spark innovation in all areas.

References

(1) Jensen, K. F., Microreaction engineering -- is small better? *Chem. Eng. Sci.* **2001,** 56, (2), 293-303.

(2) Hessel, V., Novel Process Windows – Gate to Maximizing Process Intensification via Flow Chemistry. *Chemical Engineering & Technology* **2009,** 32, (11), 1655-1681.

(3) Hartman, R. L.; McMullen, J. P.; Jensen, K. F., Deciding Whether To Go with the Flow: Evaluating the Merits of Flow Reactors for Synthesis. *Angew. Chem. Int. Ed.* **2011,** 50, (33), 7502-7519.

(4) Ratner, D. M.; Murphy, E. R.; Jhunjhunwala, M.; Snyder, D. A.; Jensen, K. F.; Seeberger, P. H., Microreactor-based reaction optimization in organic chemistry-glycosylation as a challenge. *Chem. Commun.* **2005,** 0, (5), 578-580.

(5) Zaborenko, N.; Murphy, E. R.; Kralj, J. G.; Jensen, K. F., Synthesis and Kinetics of Highly Energetic Intermediates by Micromixers: Direct Multistep Synthesis of Sodium Nitrotetrazolate. *Ind. Eng. Chem. Res.* **2010,** 49, (9), 4132-4139.

(6) Wegner, J.; Ceylan, S.; Kirschning, A., Ten key issues in modern flow chemistry. *Chem. Commun.* **2011,** 47, (16), 4583-4592.

(7) Malet-Sanz, L.; Susanne, F., Continuous Flow Synthesis. A Pharma Perspective. *J. Med. Chem.* **2012,** 55, (9), 4062-4098.

(8) Roberge, D. M.; Ducry, L.; Bieler, N.; Cretton, P.; Zimmermann, B., Microreactor Technology: A Revolution for the Fine Chemical and Pharmaceutical Industries? *Chemical Engineering & Technology* **2005,** 28, (3), 318-323.

(9) Kuhn, S.; Noel, T.; Gu, L.; Heider, P. L.; Jensen, K. F., A Teflon microreactor with integrated piezoelectric actuator to handle solid forming reactions. *Lab Chip* **2011,** 11, (15), 2488-2492.

(10) Thorsen, T.; Maerkl, S. J.; Quake, S. R., Microfluidic Large-Scale Integration. *Science* **2002,** 298, (5593), 580-584.

(11) Pal, R.; Yang, M.; Lin, R.; Johnson, B. N.; Srivastava, N.; Razzacki, S. Z.; Chomistek, K. J.; Heldsinger, D. C.; Haque, R. M.; Ugaz, V. M.; Thwar, P. K.; Chen, Z.; Alfano, K.; Yim, M. B.; Krishnan, M.; Fuller, A. O.; Larson, R. G.; Burke, D. T.; Burns, M. A., An integrated microfluidic device for influenza and other genetic analyses. *Lab Chip* **2005,** 5, (10), 1024-1032.

(12) Blazej, R. G.; Kumaresan, P.; Mathies, R. A., Microfabricated bioprocessor for integrated nanoliter-scale Sanger DNA sequencing. *Proc. Natl. Acad. Sci.* **2006,** 103, (19), 7240-7245.

(13) Webb, D.; Jamison, T. F., Continuous flow multi-step organic synthesis. *Chem. Sci.* **2010,** 1, (6), 675-680.

(14) Kralj, J. G.; Sahoo, H. R.; Jensen, K. F., Integrated continuous microfluidic liquid-liquid extraction. *Lab Chip* **2007,** 7, (2), 256-263.

(15) Sahoo, H. R.; Kralj, J. G.; Jensen, K. F., Multistep Continuous-Flow Microchemical Synthesis Involving Multiple Reactions and Separations. *Angew. Chem. Int. Ed.* **2007,** 46, (30), 5704-5708.

(16) Cervera-Padrell, A. E.; Morthensen, S. T.; Lewandowski, D. J.; Skovby, T.; Kiil, S.; Gernaey, K. V., Continuous Hydrolysis and Liquid–Liquid Phase Separation of an Active Pharmaceutical Ingredient Intermediate Using a Miniscale Hydrophobic Membrane Separator. *Org. Process Res. Dev.* **2012,** 16, (5), 888-900.

(17) Schuur, B.; Floure, J.; Hallett, A. J.; Winkelman, J. G. M.; deVries, J. G.; Heeres, H. J., Continuous Chiral Separation of Amino Acid Derivatives by Enantioselective Liquid−Liquid Extraction in Centrifugal Contactor Separators. *Org. Process Res. Dev.* **2008,** 12, (5), 950-955.

(18) Schuur, B.; Hallett, A. J.; Winkelman, J. G. M.; de Vries, J. G.; Heeres, H. J., Scalable Enantioseparation of Amino Acid Derivatives Using Continuous Liquid−Liquid Extraction in a Cascade of Centrifugal Contactor Separators. *Org. Process Res. Dev.* **2009,** 13, (5), 911-914.

(19) O'Brien, M.; Koos, P.; Browne, D. L.; Ley, S. V., A prototype continuous-flow liquid-liquid extraction system using open-source technology. *Org. Biomol. Chem.* **2012,** 10, (35), 7031-7036.

(20) Hu, D. X.; O'Brien, M.; Ley, S. V., Continuous Multiple Liquid–Liquid Separation: Diazotization of Amino Acids in Flow. *Org. Lett.* **2012,** 14, (16), 4246-4249.

(21) DiMasi, J. A.; Hansen, R. W.; Grabowski, H. G., The price of innovation: new estimates of drug development costs. *J. Health Econ.* **2003,** 22, (2), 151-185.

(22) Suresh, P.; Basu, P., Improving Pharmaceutical Product Development and Manufacturing: Impact on Cost of Drug Development and Cost of Goods Sold of Pharmaceuticals. *J. Pharm. Innov.* **2008,** 3, (3), 175-187.

(23) Federsel, H.-J., Logistics of process R&D: transforming laboratory methods to manufacturing scale. *Nature Reviews Drug Discovery* **2003,** 2, (8), 654-664.

(24) Federsel, H.-J. r., Chemical Process Research and Development in the 21st Century: Challenges, Strategies, and Solutions from a Pharmaceutical Industry Perspective. *Acc. Chem. Res.* **2009,** 42, (5), 671-680.

(25) Poechlauer, P.; Manley, J.; Broxterman, R.; Gregertsen, B.; Ridemark, M., Continuous Processing in the Manufacture of Active Pharmaceutical Ingredients and Finished Dosage Forms: An Industry Perspective. *Org. Process Res. Dev.* **2012,** 16, (10), 1586-1590.

(26) Jiménez-González, C.; Poechlauer, P.; Broxterman, Q. B.; Yang, B.-S.; am Ende, D.; Baird, J.; Bertsch, C.; Hannah, R. E.; Dell'Orco, P.; Noorman, H.; Yee, S.; Reintjens, R.; Wells, A.; Massonneau, V.; Manley, J., Key Green Engineering Research Areas for Sustainable Manufacturing: A Perspective from Pharmaceutical and Fine Chemicals Manufacturers. *Org. Process Res. Dev.* **2011,** 15, (4), 900-911.

(27) Johnson, M. D.; May, S. A.; Calvin, J. R.; Remacle, J.; Stout, J. R.; Diseroad, W. D.; Zaborenko, N.; Haeberle, B. D.; Sun, W.-M.; Miller, M. T.; Brennan, J., Development and Scale-Up of a Continuous, High-Pressure, Asymmetric Hydrogenation Reaction, Workup, and Isolation. *Org. Process Res. Dev.* **2012,** 16, (5), 1017-1038.

(28) Wiles, C.; Watts, P., Recent advances in micro reaction technology. *Chem. Commun.* **2011,** 47, (23), 6512-6535.

(29) Pennemann, H.; Watts, P.; Haswell, S. J.; Hessel, V.; Löwe, H., Benchmarking of Microreactor Applications. *Org. Process Res. Dev.* **2004,** 8, (3), 422-439.

(30) Kockmann, N.; Gottsponer, M.; Zimmermann, B.; Roberge, D. M., Enabling Continuous-Flow Chemistry in Microstructured Devices for Pharmaceutical and Fine-Chemical Production. *Chem. Eur. J.* **2008,** 14, (25), 7470-7477.

(31) Battilocchio, C.; Baumann, M.; Baxendale, I. R.; Biava, M.; Kitching, M. O.; Ley, S. V.; Martin, R. E.; Ohnmacht, S. A.; Tappin, N. D. C., Scale-Up of Flow-Assisted Synthesis of C2-Symmetric Chiral PyBox Ligands. *Synthesis* **2012,** 2012, (04), 635-647.

(32) McMullen, J. P.; Jensen, K. F., Rapid Determination of Reaction Kinetics with an Automated Microfluidic System. *Org. Process Res. Dev.* **2011,** 15, (2), 398-407.

(33) Cervera-Padrell, A. E.; Nielsen, J. P.; Jønch Pedersen, M.; Müller Christensen, K.; Mortensen, A. R.; Skovby, T.; Dam-Johansen, K.; Kiil, S.; Gernaey, K. V., Monitoring and Control of a Continuous Grignard Reaction for the Synthesis of an Active Pharmaceutical Ingredient Intermediate Using Inline NIR spectroscopy. *Org. Process Res. Dev.* **2012,** 16, (5), 901-914.

(34) Kockmann, N.; Gottsponer, M.; Roberge, D. M., Scale-up concept of single-channel microreactors from process development to industrial production. *Chem. Eng. J.* **2011,** 167, (2–3), 718-726.

(35) Hessel, V.; Löb, P.; Löwe, H., Industrial Microreactor Process Development up to Production. In *Microreactors in Organic Synthesis and Catalysis*, Wiley-VCH Verlag GmbH & Co. KGaA: 2008; pp 211-275.

(36) Smith, C. J.; Nikbin, N.; Ley, S. V.; Lange, H.; Baxendale, I. R., A fully automated, multistep flow synthesis of 5-amino-4-cyano-1,2,3-triazoles. *Org. Biomol. Chem.* **2011,** 9, (6), 1938-1947.

(37) Bogdan, A. R.; Poe, S. L.; Kubis, D. C.; Broadwater, S. J.; McQuade, D. T., The Continuous-Flow Synthesis of Ibuprofen. *Angew. Chem. Int. Ed.* **2009,** 48, (45), 8547-8550.

(38) Varas, A. C.; Noël, T.; Wang, Q.; Hessel, V., Copper(I)-Catalyzed Azide–Alkyne Cycloadditions in Microflow: Catalyst Activity, High-T Operation, and an Integrated Continuous Copper Scavenging Unit. *ChemSusChem* **2012,** 5, (9), 1703-1707.

(39) Hartman, R. L.; Naber, J. R.; Buchwald, S. L.; Jensen, K. F., Multistep Microchemical Synthesis Enabled by Microfluidic Distillation. *Angew. Chem. Int. Ed.* **2010,** 49, (5), 899-903.

(40) Tzschucke, C. C.; Markert, C.; Bannwarth, W.; Roller, S.; Hebel, A.; Haag, R., Modern Separation Techniques for the Efficient Workup in Organic Synthesis. *Angew. Chem. Int. Ed.* **2002,** 41, (21), 3964-4000.

(41) Kuhn, S.; Jensen, K. F., A pH-Sensitive Laser-Induced Fluorescence Technique To Monitor Mass Transfer in Multiphase Flows in Microfluidic Devices. *Ind. Eng. Chem. Res.* **2012,** 51, (26), 8999-9006.

(42) Burns, J. R.; Ramshaw, C., The intensification of rapid reactions in multiphase systems using slug flow in capillaries. *Lab Chip* **2001,** 1, (1), 10-15.

(43) Günther, A.; Jensen, K. F., Multiphase microfluidics: from flow characteristics to chemical and materials synthesis. *Lab Chip* **2006,** 6, (12), 1487-1503.

(44) Aota, A.; Nonaka, M.; Hibara, A.; Kitamori, T., Countercurrent Laminar Microflow for Highly Efficient Solvent Extraction. *Angew. Chem. Int. Ed.* **2007,** 46, (6), 878-880.

(45) Aota, A.; Mawatari, K.; Kitamori, T., Parallel multiphase microflows: fundamental physics, stabilization methods and applications. *Lab Chip* **2009,** 9, (17), 2470-2476.

(46) Aota, A.; Mawatari, K.; Takahashi, S.; Matsumoto, T.; Kanda, K.; Anraku, R.; Hibara, A.; Tokeshi, M.; Kitamori, T., Phase separation of gas–liquid and liquid–liquid microflows in microchips. *Microchim. Acta* **2009,** 164, (3), 249-255.

(47) Castell, O. K.; Allender, C. J.; Barrow, D. A., Liquid-liquid phase separation: characterisation of a novel device capable of separating particle carrying multiphase flows. *Lab Chip* **2009,** 9, (3), 388-396.

(48) Kashid, M. N.; Harshe, Y. M.; Agar, D. W., Liquid−Liquid Slug Flow in a Capillary: An Alternative to Suspended Drop or Film Contactors. *Ind. Eng. Chem. Res.* **2007,** 46, (25), 8420-8430.

(49) Peroni, D.; van Egmond, W.; Kok, W. T.; Janssen, H.-G., Advancing liquid/liquid extraction through a novel microfluidic device: Theory, instrumentation and applications in gas chromatography. *J. Chromatogr. A* **2012,** 1226, (0), 77-86.

(50) Hartman, R. L.; Sahoo, H. R.; Yen, B. C.; Jensen, K. F., Distillation in microchemical systems using capillary forces and segmented flow. *Lab Chip* **2009,** 9, (13), 1843-1849.

(51) Perry, R. H.; Green, D. W., *Perry's Chemical Engineers' Handbook*. Seventh ed.; McGraw-Hill: New York, USA, 1997; p. 6-12.

(52) Donahue, D. J.; Bartell, F. E., The Boundary Tension at Water-Organic Liquid Interfaces. *J. Phys. Chem.* **1952,** 56, (4), 480-484.

(53) Seader, J. D.; Henley, E. J., *Separation Process Principles*. 2nd ed.; John Wiley & Sons, Inc.: 2006.

(54) Lam, K. F.; Cao, E.; Sorensen, E.; Gavriilidis, A., Development of multistage distillation in a microfluidic chip. *Lab Chip* **2011,** 11, (7), 1311-1317.

(55) Zhang, Y.; Kato, S.; Anazawa, T., Vacuum membrane distillation by microchip with temperature gradient. *Lab Chip* **2010,** 10, (7), 899-908.

(56) Sheldon, R. A., The E Factor: fifteen years on. *Green Chem.* **2007,** 9, (12), 1273-1283.

(57) Evans, J., A Paradigm Shift. *The Chem. Eng.* **2013**, (860), 32-34.

(58) Roberge, D. M.; Zimmermann, B.; Rainone, F.; Gottsponer, M.; Eyholzer, M.; Kockmann, N., Microreactor Technology and Continuous Processes in the Fine Chemical and Pharmaceutical Industry: Is the Revolution Underway? *Org. Process Res. Dev.* **2008,** 12, (5), 905-910.

(59) Benaskar, F.; Ben-Abdelmoumen, A.; Patil, N.; Rebrov, E.; Meuldijk, J.; Hulshof, L.; Hessel, V.; Krtschil, U.; Schouten, J., Cost Analysis for a Continuously Operated Fine Chemicals Production Plant at 10 Kg/Day Using a Combination of Microprocessing and Microwave Heating. *J. Flow Chem.* **2011,** 1, (2), 74-89.

(60) Schaber, S. D.; Gerogiorgis, D. I.; Ramachandran, R.; Evans, J. M. B.; Barton, P. I.; Trout, B. L., Economic Analysis of Integrated Continuous and Batch Pharmaceutical Manufacturing: A Case Study. *Ind. Eng. Chem. Res.* **2011,** 50, (17), 10083-10092.

(61) Jimenez, J., A Defining Moment: The Future of Manufacturing in the US. In *The Future of Manufacturing in the U.S.*, Cambridge, MA, USA, 2012.

(62) Wu, H.; Khan, M. A.; Hussain, A. S., Process Control Perspective for Process Analytical Technology: Integration of Chemical Engineering Practice into Semiconductor and Pharmaceutical Industries. *Chem. Eng. Commun.* **2007,** 194, (6), 760-779.

(63) Lionberger, R.; Lee, S.; Lee, L.; Raw, A.; Yu, L., Quality by Design: Concepts for ANDAs. *AAPS J.* **2008,** 10, (2), 268-276.

(64) Cervera-Padrell, A. E.; Skovby, T.; Kiil, S.; Gani, R.; Gernaey, K. V., Active pharmaceutical ingredient (API) production involving continuous processes – A process system engineering (PSE)-assisted design framework. *Eur. J. Pharm. Biopharm.* **2012,** 82, (2), 437-456.

(65) Benyahia, B.; Lakerveld, R.; Barton, P. I., A Plant-Wide Dynamic Model of a Continuous Pharmaceutical Process. *Ind. Eng. Chem. Res.* **2012,** 51, (47), 15393-15412.

(66) Boukouvala, F.; Niotis, V.; Ramachandran, R.; Muzzio, F. J.; Ierapetritou, M. G., An integrated approach for dynamic flowsheet modeling and sensitivity analysis of a continuous tablet manufacturing process. *Comput. Chem. Eng.* **2012,** 42, (0), 30-47.

(67) Baumann, M.; Baxendale, I. R.; Ley, S. V.; Nikbin, N.; Smith, C. D.; Tierney, J. P., A modular flow reactor for performing Curtius rearrangements as a continuous flow process. *Org. Biomol. Chem.* **2008,** 6, (9), 1577-1586.

(68) Pollet, P.; Cope, E. D.; Kassner, M. K.; Charney, R.; Terett, S. H.; Richman, K. W.; Dubay, W.; Stringer, J.; Eckert, C. A.; Liotta, C. L., Production of (S)-1-Benzyl-3-diazo-2-oxopropylcarbamic Acid tert-Butyl Ester, a Diazoketone Pharmaceutical Intermediate, Employing a Small Scale Continuous Reactor. *Ind. Eng. Chem. Res.* **2009,** 48, (15), 7032-7036.

(69) Christensen, K. M.; Pedersen, M. J.; Dam-Johansen, K.; Holm, T. L.; Skovby, T.; Kiil, S., Design and operation of a filter reactor for continuous production of a selected pharmaceutical intermediate. *Chem. Eng. Sci.* **2012,** 71, (0), 111-117.

(70) Chen, J.; Sarma, B.; Evans, J. M. B.; Myerson, A. S., Pharmaceutical Crystallization. *Cryst. Growth Des.* **2011,** 11, (4), 887-895.

(71) Lawton, S.; Steele, G.; Shering, P.; Zhao, L.; Laird, I.; Ni, X.-W., Continuous Crystallization of Pharmaceuticals Using a Continuous Oscillatory Baffled Crystallizer. *Org. Process Res. Dev.* **2009,** 13, (6), 1357-1363.

(72) Griffin, D. W.; Mellichamp, D. A.; Doherty, M. F., Reducing the mean size of API crystals by continuous manufacturing with product classification and recycle. *Chem. Eng. Sci.* **2010,** 65, (21), 5770-5780.

(73) Eder, R. J. P.; Schmitt, E. K.; Grill, J.; Radl, S.; Gruber-Woelfler, H.; Khinast, J. G., Seed loading effects on the mean crystal size of acetylsalicylic acid in a continuous-flow crystallization device. *Cryst. Res. Technol.* **2011,** 46, (3), 227-237.

(74) Wong, S. Y.; Tatusko, A. P.; Trout, B. L.; Myerson, A. S., Development of Continuous Crystallization Processes Using a Single-Stage Mixed-Suspension, Mixed-Product Removal Crystallizer with Recycle. *Cryst. Growth Des.* **2012,** 12, (11), 5701-5707.

(75) Gonnissen, Y.; Gonçalves, S. I. V.; De Geest, B. G.; Remon, J. P.; Vervaet, C., Process design applied to optimise a directly compressible powder produced via a continuous manufacturing process. *Eur. J. Pharm. Biopharm.* **2008,** 68, (3), 760-770.

(76) Wang, M.; Rutledge, G. C.; Myerson, A. S.; Trout, B. L., Production and characterization of carbamazepine nanocrystals by electrospraying for continuous pharmaceutical manufacturing. *J. Pharm. Sci.* **2012,** 101, (3), 1178-1188.

(77) Brettmann, B.; Cheng, K.; Myerson, A.; Trout, B., Electrospun Formulations Containing Crystalline Active Pharmaceutical Ingredients. *Pharm. Res.* **2013,** 30, (1), 238-246.

(78) Pernenkil, L.; Cooney, C. L., A review on the continuous blending of powders. *Chem. Eng. Sci.* **2006,** 61, (2), 720-742.

(79) Portillo, P. M.; Ierapetritou, M. G.; Muzzio, F. J., Characterization of continuous convective powder mixing processes. *Powder Technol.* **2008,** 182, (3), 368-378.

(80) Dubey, A.; Vanarase, A. U.; Muzzio, F. J., Impact of process parameters on critical performance attributes of a continuous blender—A DEM-based study. *AIChE J.* **2012,** 58, (12), 3676-3684.

(81) Järvinen, K.; Hoehe, W.; Järvinen, M.; Poutiainen, S.; Juuti, M.; Borchert, S., In-line monitoring of the drug content of powder mixtures and tablets by near-infrared spectroscopy during the continuous direct compression tableting process. *Eur. J. Pharm. Sci.* **2013,** 48, (4–5), 680-688.

(82) Keleb, E. I.; Vermeire, A.; Vervaet, C.; Remon, J. P., Cold extrusion as a continuous single-step granulation and tabletting process. *Eur. J. Pharm. Biopharm.* **2001,** 52, (3), 359-368.

(83) Djuric, D.; Van Melkebeke, B.; Kleinebudde, P.; Remon, J. P.; Vervaet, C., Comparison of two twin-screw extruders for continuous granulation. *Eur. J. Pharm. Biopharm.* **2009,** 71, (1), 155-160.

(84) Singh, R.; Ierapetritou, M.; Ramachandran, R., An engineering study on the enhanced control and operation of continuous manufacturing of pharmaceutical tablets via roller compaction. *Int. J. Pharm.* **2012,** 438, (1–2), 307-326.

(85) Sen, M.; Chaudhury, A.; Singh, R.; John, J.; Ramachandran, R., Multi-scale flowsheet simulation of an integrated continuous purification–downstream pharmaceutical manufacturing process. *Int. J. Pharm.* **2013,** 445, (1–2), 29-38.

(86) Based on the process used by Novartis.

(87) Foley, M. A.; Jamison, T. F., Amide Bond Formation via Reversible, Carboxylic Acid-Promoted Lactone Aminolysis. *Org. Process Res. Dev.* **2010,** 14, (5), 1177-1181.

(88) Rüeger, H.; Stutz, S.; Göschke, R.; Spindler, F.; Maibaum, J., A convergent synthesis approach towards CGP60536B, a non-peptide orally potent renin inhibitor, via an enantiomerically pure ketolactone intermediate. *Tetrahedron Lett.* **2000,** 41, (51), 10085-10089.

(89) Sandham, D. A.; Taylor, R. J.; Carey, J. S.; Fässler, A., A convergent synthesis of the renin inhibitor CGP60536B. *Tetrahedron Lett.* **2000,** 41, (51), 10091-10094.

(90) Dondoni, A.; De Lathauwer, G.; Perrone, D., A convergent synthesis of the renin inhibitor SPP-100 using a nitrone intermediate. *Tetrahedron Lett.* **2001,** 42, (29), 4819-4823.

(91) Hanessian, S.; Guesné, S.; Chénard, E., Total Synthesis of "Aliskiren": The First Renin Inhibitor in Clinical Practice for Hypertension. *Org. Lett.* **2010,** 12, (8), 1816-1819.

(92) Zhang, H.; Quon, J.; Alvarez, A. J.; Evans, J.; Myerson, A. S.; Trout, B., Development of Continuous Anti-Solvent/Cooling Crystallization Process using Cascaded Mixed Suspension, Mixed Product Removal Crystallizers. *Org. Process Res. Dev.* **2012,** 16, (5), 915-924.

(93) Lakerveld, R.; Benyahia, B.; Braatz, R. D.; Barton, P. I., Model-based design of a plant-wide control strategy for a continuous pharmaceutical plant. *AIChE J.* **2013**, DOI: 10.1002/aic.14107.

(94) Quon, J. L.; Zhang, H.; Alvarez, A.; Evans, J.; Myerson, A. S.; Trout, B. L., Continuous Crystallization of Aliskiren Hemifumarate. *Cryst. Growth Des.* **2012,** 12, (6), 3036-3044.

(95) Gold, G.; Duvall, R. N.; Palermo, B. T.; Slater, J. G., Powder flow studies II. Effect of glidants on flow rate and angle of repose. *J. Pharm. Sci.* **1966,** 55, (11), 1291-1295.

(96) Bell, E. R. Melt Extrusion and Continuous Manufacturing of Pharmaceutical Materials. PhD, MIT, USA, 2011.

(97) Breitenbach, J., Melt extrusion: from process to drug delivery technology. *Eur. J. Pharm. Biopharm.* **2002,** 54, (2), 107-117.

(98) USP <711>.

(99) ICH Q3C (R5).

(100) USP <905>.

(101) ICH Q3B(R2).

(102) Li, P.; Buchwald, S. L., Continuous-Flow Synthesis of 3,3-Disubstituted Oxindoles by a Palladium-Catalyzed α-Arylation/Alkylation Sequence. *Angew. Chem. Int. Ed.* **2011,** 50, (28), 6396-6400.

(103) The molar absorptivities of 2 and 5 differ by less than 5 %.

(104) Levenspiel, O., *Chemical Reaction Engineering*. Third ed.; John Wiley & Sons: New York, 1999.

(105) Ananthakrishnan, V.; Gill, W. N.; Barduhn, A. J., Laminar dispersion in capillaries: Part I. Mathematical analysis. *AIChE J.* **1965,** 11, (6), 1063-1072.

(106) Togkalidou, T.; Fujiwara, M.; Patel, S.; Braatz, R. D., Solute concentration prediction using chemometrics and ATR-FTIR spectroscopy. *J. Cryst. Growth* **2001,** 231, (4), 534-543.

Appendix A. Detailed process description of integrated continuous plant

All unit operation references in Appendix A correspond to Figure 16. Except for Figure 17, Figure 19, and Figure 22, all plots of data from the continuous plant use the same initial time ($t = 0$) of the point when the pumps for the beginning of the process (P1, P2, and P3) were turned on. The control system is implemented using Siemens PCS7 software. Data from the control system are recorded at a 1 s to 1 min sampling frequency into a central database. All equipment receives setpoints from the control system. The units are brought close to steady state manually and then are switched over to automated closed-loop control. Manual interventions are only made in extreme cases where significant deviations would cause hazardous situations or would significantly impair the process performance.

A.1 Upstream operation

Unless otherwise noted, all chemicals are obtained from Sigma Aldrich and are used without further purification. DI water (Milli-Q, Millipore) is used.

1 and **2** (provided by Novartis) are manually fed into two separate melting tanks (1 L jacketed vessels) as a dry white powder. The tanks are held at 130 °C, mixed with an overhead stirrer, and material is pumped out of the tanks with two heated pumps (Quizix C-5000-10K, Vindum Engineering) located in a 130 °C oven. The two streams are then pumped into a separate reactor oven (Friction-Aire, Blue M) at 100 °C where they are initially mixed in a cross fitting with a stream of **3** and then mixed with an inline, helical static mixer (3.3 mm ID tube with 27 elements). The reagents are added in a molar ratio of 1:10:1 of **1**:**2**:**3**. The mixed stream then enters an 11.7 mm ID × 25 m stainless steel tube with a residence time of 4 h at the nominal process throughput. The reactor outlet is mixed with ethyl acetate and water to achieve 12 wt% of **4** in the organic phase and 20 wt% of **2** in the aqueous phase (based on an expected yield of 90 % and conversion of 95 %). Note that the ethyl acetate is added above its flash point. The oven is designed to handle a leak of the ethyl acetate by continuously refreshing the air in the oven keeping the concentration of ethyl acetate below the lower explosion limit. The two-phase product then passes through a backpressure regulator (Swagelok) set to 7 bar and cools to near

room temperature before entering the liquid-liquid separation system. The two-phase stream is split into twelve equal branches using tees and crosses. Each of the lines to and from the separators is cut so that there are equal lengths for each separator to ensure equal distribution of flow. Each membrane separator contains 8.57 cm^2 of microporous membrane (Pall Zelfuor 1 μm) exposed to the flow channel. The outlets of the membrane separators rejoin and the pressure is controlled (EB1, Equilibar) to ≈ 700 Pa higher pressure in the aqueous stream. The aqueous phase is sent to waste while the organic phase is passed through a flow IR cell (Mettler Toledo ReactIR 15 with DS Micro Flow Cell) to monitor the concentration of **1** and **4**.

The organic phase is pumped into Cr1, a 15 L jacketed glass vessel, which is controlled at 5 °C through a chiller. Nucleation and crystal growth occur inside the crystallizer and a slurry is formed. The level is controlled to maintain a nominal 4 h residence time. The slurry is transferred into Cr2 through a peristaltic pump (Masterflex L/S) and the flow rate is controlled by a feedback control loop through the control system. The level is monitored by ultrasonic level sensors (Omega Engineering, Inc.). An anti-solvent stream (heptane) is introduced to Cr2, a 15 L jacketed glass vessel, and the flow rate of the anti-solvent is set to control the mass ratio of 1:3 of heptane:ethyl acetate. The temperature of Cr2 is set at 5 °C. At the end of the crystallization, the slurry of **4** is pumped into a custom-designed continuous filter (W1) where the crystals of **4** are filtered and washed with ethanol and ethyl acetate. The flow rate of the slurry is controlled by a similar feedback control loop to maintain a constant level corresponding to a nominal residence time of 4 h.

The wet cake out of the filter is collected in a 5 L vessel. A side stream is pumped out of the tank, through a density flow cell (Anton Paar DPRn 417) and returned to the vessel. The density reading is used to calculate the solid loading in the vessel and then control addition of ethyl acetate into the vessel to maintain a solid loading of 26.5 wt% of **4**. A peristaltic pump (Masterflex L/S) equipped with two heads then pumps the slurry into the second reactor that consists of two parallel reactors run with each pump head. The slurry stream is mixed in a tee with 16 equivalents of 37 wt% hydrochloric acid and reacted in a 4.9 m length of 40 mm ID PFA coiled tubing. At the outlet of the reactor, 25 wt% NaOH is mixed to quench the reaction. The mixing section for the quench is constructed from a PFA tee with the crude reaction product entering from the bottom through a 0.159 cm ID PFA tube that extends into the tee in the center of the channel. The NaOH flows in the side port of the tee and flows around the outside of the

tube carrying the crude reaction product. Just beyond the end of the tee is a 0.61 cm OD PTFE helical mixer (Stamixco) with 10 units. This is contained within a 0.635 cm ID tube that terminates by reducing to a 0.159 cm ID tube at the end of the static mixer. The quenched stream passes through a pH flow cell (Hamilton Polilyte Plus) that is used in a feedback control loop to adjust the NaOH flow rate to maintain a pH of 12. Control is implemented as a proportional-integral controller with a gain of 27 mL h^{-1} and an integral time constant of 50 s.

The two phase reaction product is sent into a 2 L settling tank where the bottom aqueous phase is pumped to waste while the top organic phase with **5** is pumped out into a mixing tee to mix with ethyl acetate controlled by a UV flow cell located downstream. The stream (containing solid NaCl that precipitates after dilution) is then filtered through 14 microfiltration membranes (0.45 μm Pellicon XL 50, Millipore). After filtration, the stream passes through a UV flow cell (HR2000+, Ocean Optics) that feeds back the concentration of **5** to the dilution pump prior to the microfiltration membranes. The concentration is maintained at 6 wt%. The organic stream then passes through 2 × 35 L packed columns of 3 Å molecular sieves in series to remove any residual water that is present in the stream. The size of the column is selected such that it will contain all of the water for a given run (up to two weeks of operation). Continuous operation could be enabled by switching between smaller columns run in parallel. The stream then exits the column into a break tank where it is metered into the next crystallization process. It passes through another UV flow cell where the concentration of **5** is again measured and fed forward to control the pump delivering fumaric acid into Cr3, a 15 L jacketed glass vessel.

The reagents are fed in a molar ratio of 0.55:1 of fumaric acid:**5**. The temperature in Cr3 is controlled at 20 °C. The salt formation reaction and the crystallization of the final drug substance occur in Cr3 at the same time. The slurry is transferred into Cr4, another 15 L jacketed glass vessel, with a peristaltic pump (Masterflex L/S) and the flow rate is controlled by a feedback control loop through the control system to maintain a level corresponding to a nominal residence time of 4 h. The temperature of Cr4 is controlled at −10 °C. At the end of the crystallization, the slurry of the final drug substance is pumped into another continuous filter (W2) where the crystals are filtered and washed with ethyl acetate. The flow rate of the slurry is controlled by the feedback level control loop in Cr4 to maintain a nominal residence time of 4 h.

The wet cake out of the filter is collected in a 5 L vessel. A side stream is pumped out of the tank, through a density flow cell (Anton Paar DPRn 417) and returned to the vessel. The

density reading is used to calculate the solid loading in the vessel and then control addition of ethyl acetate into the vessel to maintain a solid loading between 10–15 wt% **6**. A peristaltic pump (Masterflex L/S) then pumps the slurry into the continuous dryer. A second pump meters a 2.5 wt% slurry of fumed SiO_2 (Sigma-Aldrich #S5505) such that the mixture with the **6** slurry is 2.5 wt% SiO_2 on a dry basis.

A.2 Downstream operation

The continuous dryer combines a rotary drum dryer and a screw vacuum dryer. The drum dryer includes two horizontal, stainless steel, hollow drums (21.6 cm diameter) rotating at 50 rpm in opposite directions relative to each other. The product is pumped between a 0.1 mm gap between the drums, where it is squeezed while 95 °C air is blown on the product surface of the back side of the drum. The semidried wetcake is broken down into particulates by the action of static stainless steel scraper blades located on the either side of each drum. Particles fall into a hopper that vibrates in order to release the material through a butterfly valve into an airlock before entering a 3-zone vacuum screw dryer. The vacuum screw dryer consists of 3 sections of 6 cm ID × 1.5 m long pipe with acetal screws. The temperature zones in the dryer are controlled at sequentially higher temperatures of 40 °C, 60 °C, and 75 °C. The material is conveyed down the pipes by the auger-type screws. The vacuum level within the screw dryer is < 30 mTorr.

A vacuum conveyor (IEDCO) activates automatically every 2 minutes for 20 seconds to transport the dry API powder into a reservoir (≈ 100 g capacity) located at the top of a gravimetric feeder for the API. Two gravimetric feeders (Schenk AccuRate PureFeed DP-4) supply the API and the excipient material directly into an extruder at a rate of 45 g h^{-1} and 85 g h^{-1}, respectively. The excipient is 6,000 Da polyethylene glycol (PEG, Sigma-Aldrich #81260). The co-rotating screws inside the extruder (Leistritz, 16 mm twin screw extruder) rotate at 160 rpm while mixing and pushing material through five temperature-controlled zones. The first acts as the cooling zone to prevent build-up of API or excipient in the extruder hopper and is set at 16 °C, while the remaining four zones are set at 60 °C. The average extruder residence time at steady-state is around 12 minutes.

The extrudate is continuously fed into an integrated hot-runner molding system (Mold Hot Runner Solutions). The molding unit consists of two heated reservoirs (90 °C), a heated manifold (90 °C), and a heated valve gate region (T = 90 °C). As the material is ejected through

the manifold via an injection piston, it travels through the heated valve gates into six cavities that are continuously chilled to approximately 0 °C. The material is cooled for 36 s and the tablets are then ejected via a stripper plate mechanism from the cavities.

Tablet coating is performed using a continuous dip coating setup where tablets are pneumatically conveyed into a hopper that loads individual tablets down a chute individually. Tweezers grab a tablet and dip it into a heated bath (65 °C) and then lift the tablet out. The coating formulation is 90 wt% PEG 4,000 Da and 10 wt% OpaDry AMB (Colorcon). The coated tablet is then lifted out and held briefly over a 1.5 m forced air cooling column where the tablet is dropped and cools as it descends down the tube.

A.3 Online concentration measurements

Three different techniques are used to monitor concentration online. While HPLC is extremely accurate and able to detect small (≈ 0.1 %) levels of impurities, it is slow requiring 5 min to prepare a sample and 10-30 min to run the sample. This is too slow for feedback or feedforward control of some of the streams. Three different online concentration measurements are used to supplement HPLC: FTIR, density, and UV.

A.3.1 Complex solution composition monitoring by FTIR

A Mettler Toledo React IR 15 with a flow cell containing a SiComp silicon window is located at CT1 (Figure 16). The stream is a complex mixture with **1**, **4**, water, and other smaller amounts of impurities dissolved in ethyl acetate. Characteristic traces for **1** and **4** in ethyl acetate are shown in Figure 33. The ethyl acetate spectrum completely dominates the signal for both **1** and **4**, but some peaks are visible. The peak pointed out by A corresponds to N-H single bond stretching in amides which would be present in **4** while B and C both correspond to carbonyl stretching with the higher wavenumber shifted peak typical for 5 member lactones and lower shifted for secondary amides. The presence of the carbonyl peak in ethyl acetate introduces too much noise, however, to use these single peaks for calibration.

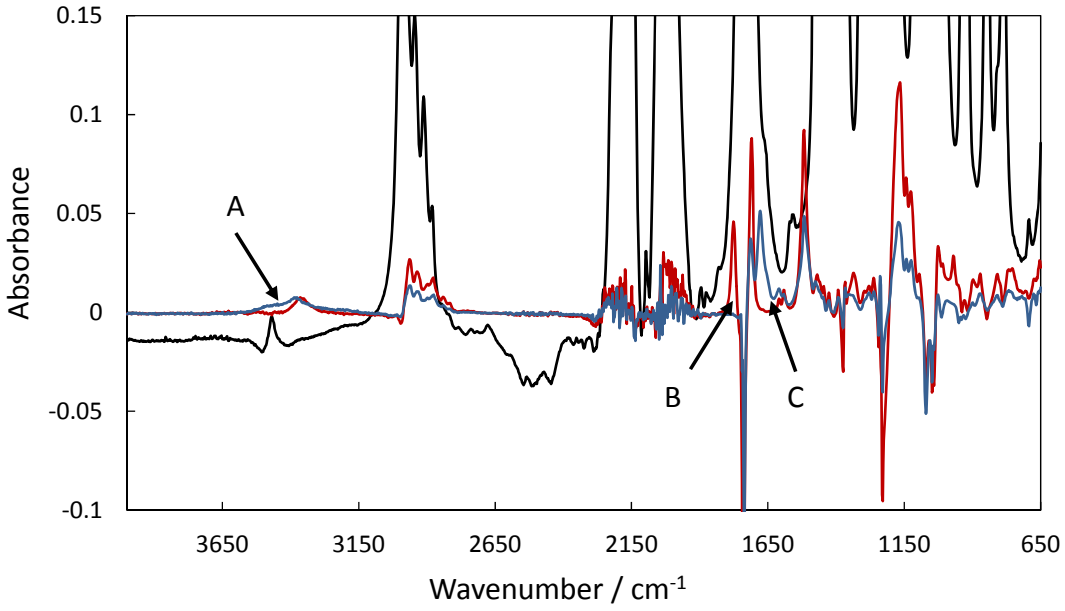

Figure 33. FTIR absorbance spectrums for species of interest. Black line is pure ethyl acetate; red line is **1** dissolved in ethyl acetate with the ethyl acetate spectrum subtracted out; blue line is **4** dissolved in ethyl acetate with the ethyl acetate spectrum subtracted out.

Multivariate models would improve calibration by monitoring lateral shifts in peaks and shoulders that form.[106] Siemens provides a package called SIPAT which is designed to integrate natively with various process analytical technologies (PAT) such as FTIR devices. It would take in the entire IR spectrum and be able to perform mathematical transformations on it to extract concentration data. This software did not function properly due to complications in setting up Windows user accounts permissions on the multiple computers in the control system network. Mettler Toledo's software provides a multivariate package for modeling which was used for both **1** and **4**. Unfortunately, the model is hidden in the software, but the parameters used to construct it are able to be adjusted by the user. The model for **1** uses two factors and three regions each with its own two-point baseline and operates on a differentiated spectrum (first derivative, based on an air blank). The model for **4** uses three factors and three regions each with a separate two-point baseline and operates on the native spectrum (based on an air blank). Table 8 summarizes the regions used. The fit is not great, however, as seen in Figure 34. The absolute value for the FTIR measurement is off and shows a dome trend not observed in the HPLC data. The disturbances at 180 h and near the end do show up, but have the opposite signs making the FTIR

data only good for monitoring large upsets. The measurement is also slow as a one minute average of spectrums is required to obtain low noise. Significant work is required to make a model for accurately monitoring the composition of this stream by FTIR.

Table 8. IR calibration ranges for multivariate model

Species	Region	Region range / cm^{-1}	Baseline range / cm^{-1}
1	1	1495-1540	1414-1580
	2	1672-1778	1610-1820
	3	2855-3017	2855-3044
4	1	1137-1182	1137-1182
	2	1497-1532	1497-1532
	3	1565-1689	1565-1689

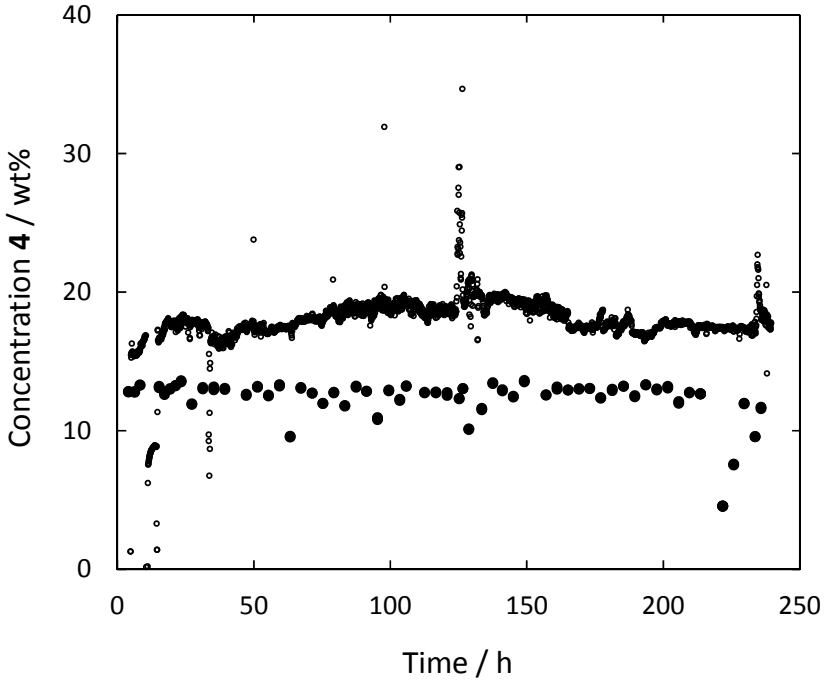

Figure 34. IR (small, open circles) and HPLC (large, filled circles) measurements of the concentration of **4** exiting S1

A.3.2 Monitoring of slurry concentration by densitometer

After each filtration (Figure 16, W1 and W2), the resulting slurry needed to be resuspended at the correct concentration. This required mixing the wet cake in a vessel while adding solvent. The high solid loading required, > 10 wt%, meant that the slurry is too thick to

measure by turbidity. The slurry is high purity meaning there are only two components, the solvent and solid. This means it can be described by two properties, density and temperature in this case. The resulting model has a simple, linear form:

$$C = a \cdot T + b \cdot \rho + c \tag{13}$$

where C is the total concentration of the species of interest, T is the temperature, ρ is the density, and a, b, and c are fitted parameters. The values for the fitted parameters are given in Table 9. Figure 35 shows the parity plot for the model fit for **4** in D1.

Table 9. Model parameters for density calibration for CC1 and CC4[a]

Parameter	D1	D2
a	0.52	0.57
b	466.88	473.46
c	-428.33	-438.52

[a]Using Equation (13) with C in wt%, T in °C, and ρ in g mL^{-1}.

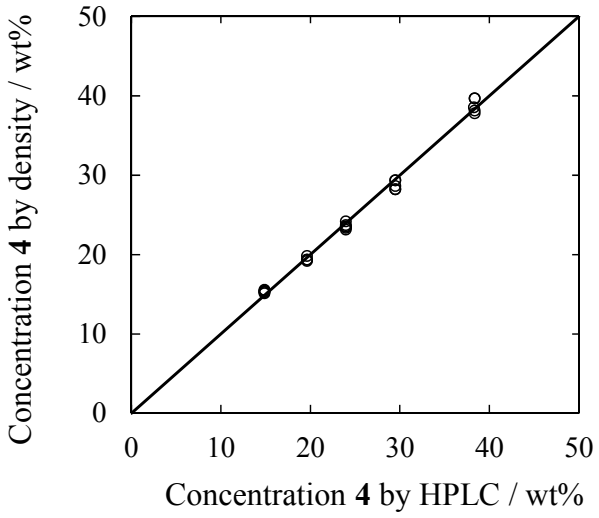

Figure 35. Parity plot for densitometer measurement of concentration compared to concentration by HPLC.

The performance of the model for the slurry in D1 (Figure 16) is shown in Figure 36. While the density measurement does show some response by decreasing initially as the tank is diluted and increasing when the setpoint is raised around 40 h, it does not accurately track the HPLC values. Samples for HPLC are collected from the exit of the densitometer side loop to

ensure the sample is the same as that measured by the densitometer; however, accurately manipulating the sample to get a characteristic sample for dilution with the HPLC solvent is difficult. This would explain some of the large scatter observed in the HPLC data and may explain some of the lack of correlation between the two measurements. The density correlation is also highly sensitive to impurities. Small amounts of water will greatly change the solubility of the solid which will dissolve more solid and shift the density. While the density measurement itself is rapid, it takes minutes to flush out the side loop as the pump running the loop is limited on the maximum flow rate. Too high a flow rate in the side loop causes gas entrainment or formation (degassing from pressure drop in line) which greatly disturbs the density measurement. Overall, the density measurement works for crude measurements of concentration, but cannot be trusted for accuracy. This is sufficient for this continuous process as the concentration control is primarily to ensure the slurry is dilute enough to be pumpable without being too thin for the subsequent unit operation.

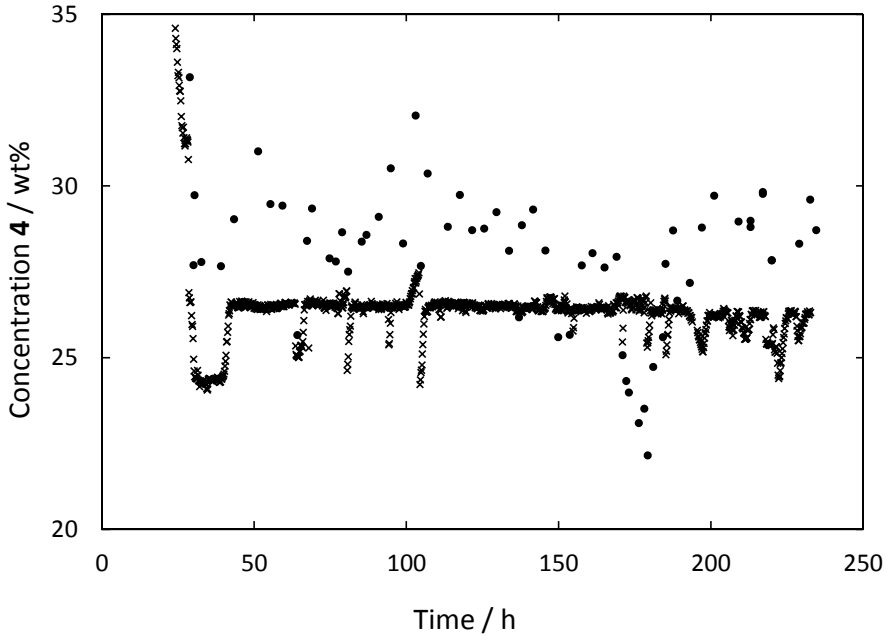

Figure 36. Density (crosses) and HPLC (circles) measurements of the concentration of **4** within D1. Density measurements are median values taken in 10 min intervals of 10 s samples.

A.3.3 Online UV monitoring for accurate concentration measurement

The last online concentration measurement used in the continuous process is a UV absorption flow cell (Figure 16, CC3 and CT2) used to monitor **5**. The absorption of ethyl acetate and **5** overlaps at lower wavelengths so the spectrometer is set to monitor 300 nm, well away from the peak for **5**. Lower wavelengths result in no signal to the detector while **5** does not absorb at higher wavelengths. Operating at 300 nm provides a narrow window where the concentration can be calibrated over a relatively narrow range compared to typical uses of UV concentration measurement. Because the streams monitored are only approximately 95 % pure (by HPLC area), the calibration must be made online with material from the process to capture the effects of impurities. The low dynamic range and calibration with impurities limits the range the model can be applied to values close to the conditions used during calibration. This is less of an issue in continuous flow as the process will be operating near the steady state point compared to batch operation where concentrations and compositions change dynamically throughout the process. Figure 37 shows the performance of CT2. Initially the two measurements track each other nearly perfectly. At later times, a small error between the two values develops. Note the high value at 200 h in the UV signal is due to stopped flow in the flow cell which drained out leaving an air bubble caused by halting of the upstream flow to refill a tank that had drained. The UV signal is the fastest to respond since it measures a small volume that is in the main flow path and gathers samples at > 100 Hz for averaging. Overall, the UV measurement performed the best, although it is limited by requiring online calibration and retesting for impurity levels.

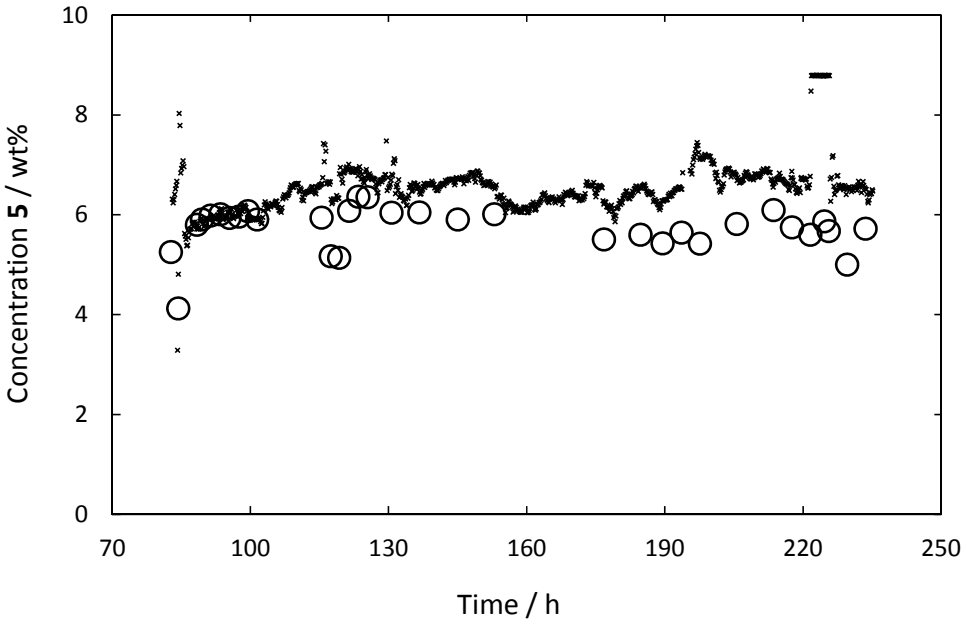

Figure 37. UV (crosses) and HPLC (open circles) measurements of the concentration of **5** entering Cr3. UV measurements are median values taken in 10 min intervals of 10 s samples.

A.4 Analysis of samples

Analytically pure samples of **1**, **2**, **4**, **5**, **6**, and **7** were provided by Novartis. Identities of compounds are confirmed by matching peaks using validated HPLC methods from Novartis (see HPLC analysis below). Concentrations of reactants, products, side products, and byproducts are monitored by HPLC (Agilent 1100). Residual solvent levels in the dried powders and final tablet are monitored by headspace GC (Agilent 7890A with a G1888 headspace sampler). Differential scanning calorimetry is performed using a TA Instruments DSC Q2000 at 10 °C min^{-1}.

Dissolution testing is carried out using a basket in an Agilent Varian VK 7025 equipped with a Cassini 10-channel fiber optic sampling system (C Technologies Inc.) in combination with an Agilent Cary 50 Bio UV spectrophotometer detection system. Tablets are dissolved in 500 mL of 0.01 M HCl maintained at 37 °C. Each tablet was placed in a rotating basket and submersed in the acid solution. The concentration of API in the vessel was measured using UV detection at 279 nm via a fiber optic probe every one minute for approximately 90 minutes total.

X-ray diffraction (XRD) patterns are recorded with a PANalytical X'Pert PRO Theta/Theta Powder X-ray Diffraction System with a Cu tube and X'Celerator high-speed detector. Tablets were broken up and portions of the center core (without coating) were selected

and further ground into a powder for measurement. Crystalline **6** is measured by drying a wet cake of **6** produced under process conditions on the bench prior to analyzing.

Stability of the tablets is tested under accelerated conditions in test chambers at 40 °C and 75 % relative humidity (ESPEC LHU-113). Tablets are stored in foil sealed plastic bottles with a plug-style desiccant. Separate bottles are used for each time point and are not returned after opening.

Water content of tablets is measured by Karl Fischer titration using a Mettler Toledo V20 volumetric KF titrator. A single, whole tablet is broken up and crushed into a powder before it was added to the testing chamber.

The value for % content is calculated dividing the amount of a material in a tablet by the declared content in the tablet (112 mg **5**). Calibrations for **7** are based on assuming the same absorptivity as **5** to match specifications provided by Novartis.

A.4.1 HPLC analysis

Streams through D1 are analyzed by injecting 3 μg of **4** (samples are diluted with 1:1 water:acetonitrile) onto an Agilent ZORBAX Eclipse XDB-C18 2.1 mm ID × 50 mm, 1.8 μm particle diameter column maintained at 30 °C. Mobile phase A was 43.8 mM H_3PO_4 in water and mobile phase B was 1:1 V V^{-1} acetonitrile:methanol. The mobile phase is changed following the gradient in Table 10 at a constant total flow rate of 0.416 mL min^{-1}. Detection is performed using UV at 230 nm. Characteristic elution times – blank: 0.35 min; **4**: 6.89 min; **1**: 8.43 min.

Table 10. Mobile phase gradient for detection of **4**

Time / min	% B
0	45
5.31	70
6.63	80
7.76	80
7.80	45
10	45

Streams through S7 are analyzed by injecting 2.26 μg of **5** or 2.5 μg of **6** (samples are diluted with 85:15 V V^{-1} water:acetonitrile) onto an Agilent Ascentis Express RP-Amide 2.1 mm ID × 50 mm, 2.7 μm particle diameter column maintained at 30 °C. Mobile phase A is 0.1 vol%

trifluoroacetic acid in water and mobile phase B is 0.05 vol% trifluoroacetic acid in acetonitrile. The mobile phase is changed following the gradient in Table 11 at a constant flow rate of 0.8 mL min^{-1}. Detection is performed using UV at 230 nm. Characteristic elution times – blank: 0.18 min; **5** and **6**: 2.96 min; **7**: 3.35 min; **4**: 4.10 min.

Table 11. Mobile phase gradient for detection of **5** or **6**

Time / min	% B
0	15
2.37	40
4.04	70
4.87	70
4.88	15
7.5	15

The final tablets are analyzed by injecting 2.8 μg of **5** (an entire tablet is diluted with 75:25 V V^{-1} water:acetonitrile) onto a YmC-Pack ODS-A 4.6 mm ID × 150 mm, 3 μm particle diameter column maintained at 30 °C. An ion pair solution is prepared (30 mM hexanesulfonic acid sodium salt monohydrate 20 mM sodium dihydrogen phosphate monohydrate in water adjusted to a pH value of 2.3 using 85 wt% phosphoric acid) and mixed 80:20 V V^{-1} ion pair solution:acetonitrile for mobile phase A and 20:80 V V^{-1} ion pair solution:acetonitrile for mobile phase B. The mobile phase is changed following the gradient in Table 12 at a constant flow rate of 0.8 mL min^{-1}. Detection is performed using UV at 280 nm. Characteristic elution times – blank: 2.1 min; **6**: 10.74 min; **7**: 13.45 min.

Table 12. Mobile phase gradient for analysis of final tablets

Time / min	% B
0	20
3	20
15	70
30	70
30.1	20
35	20

Appendix B. Details of content uniformity test for final tablets

Content uniformity was tested following US Pharmacopeial (USP) ⟨905⟩. Table 13 gives the values of % content of **6** in tablets for 26 tablets assayed during the period shown in Figure 22b. The value for % content is calculated dividing the amount of a material in a tablet by the declared content in the tablet (112 mg **5**). The standard procedure for USP ⟨905⟩ involves testing 10 random tablets from a batch; however, no batches are defined in continuous processes. The data pass the test for most sets of 10 random tablets, but the 5 tablets produced at 200 min have systemically low % content and can cause the test to fail. This is due to all having low tablet mass, nominally 0.400 g, while the composition is correct, nominally 34.1 wt% **6**. If these underfilled tablets are removed from the dataset, the test works. If all 26 tablets are subjected to the 30 tablet version of USP ⟨905⟩ with and without 4 additional random tablets selected from within the list (duplicated), then the set also passes. This is not a conservative modification to the test, but the deviation from 30 tablets is small so it is expected that a complete set would pass as well.

Table 13. Tablet % content **6** with tablet mass and wt% **6** for calculation of content uniformity

t / min	*C* / % content	*m* / g	*C* / wt%
0	102.3	0.4028	34.3
24	99.9	0.3918	34.4
24	97.9	0.3925	33.7
24	103.6	0.4017	34.8
66	96.4	0.3724	34.9
66	91.4	0.3539	34.8
66	94.3	0.3534	36.0
66	94.4	0.3652	34.9
66	89.5	0.3486	34.7
66	94.4	0.3736	34.1
100	99.0	0.3969	33.7
158	97.8	0.3949	33.4
200	88.2	0.3390	35.1
200	91.9	0.3598	34.5
200	89.0	0.3468	34.6
200	86.3	0.3372	34.5
200	85.5	0.3299	35.0
230	98.9	0.3998	33.4
277	96.5	0.3930	33.1
277	98.9	0.3807	35.1
277	97.0	0.3740	35.0
277	96.7	0.3738	34.9
277	93.1	0.3657	34.4
337	92.6	0.3994	31.3
397	96.6	0.3939	33.1

Appendix C. Construction of milliscale separators

C.1 Design 1

The initial separator design requires two identical parts (Figure 38). The membrane is cut to size and clamped between the two parts with screws. One of the outlet holes is plugged (inlet end of the permeate side).

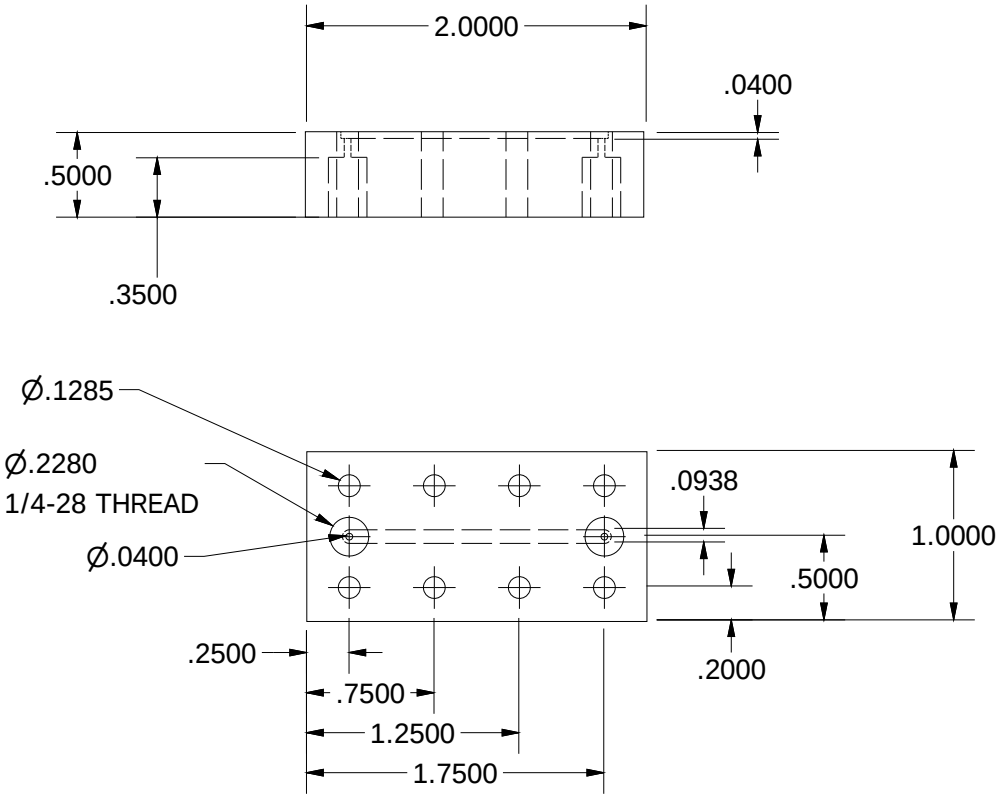

Figure 38. Drawing of half of Design 1 separator. All dimensions given in inches.

C.2 Design 2

Design 2 involves two different parts (Figure 39) clamped together around a full 47 mm membrane disk. The bottom surface is polished smooth with 400 grit sandpaper to ensure a good seal between the two faces against the membrane.

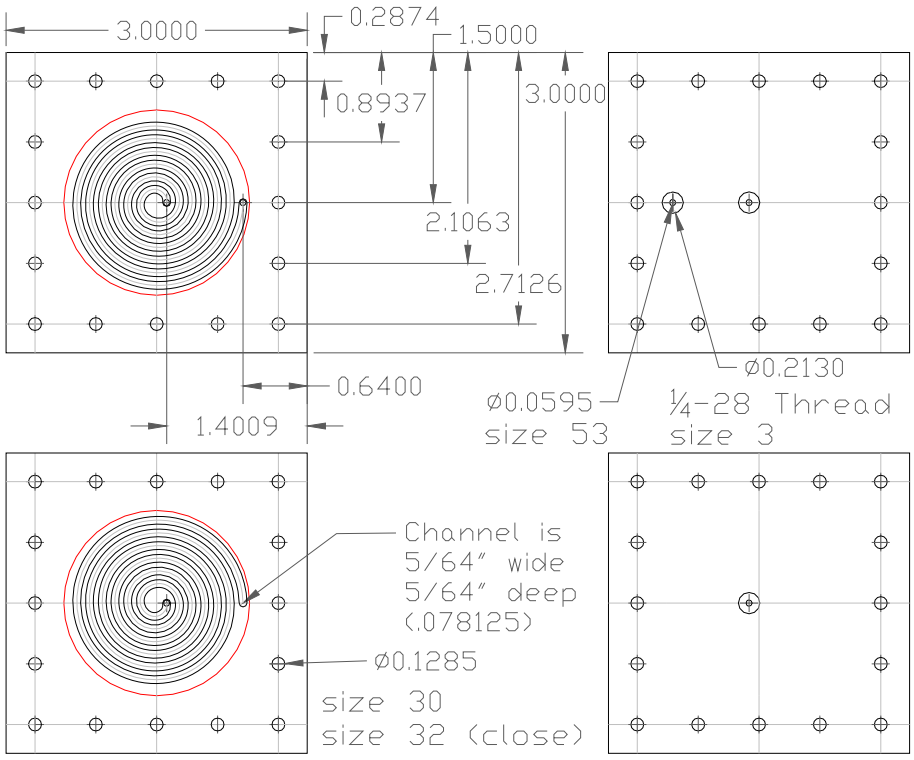

Figure 39. Design 2 drawing. Red circle shows location of membrane. All dimensions given in inches.

C.3 Design 3

Design 3 includes two different parts (Figure 40 and Figure 41). A 142 mm diameter membrane is clamped between the two raised circular sections which are polished with 400 grit sandpaper.

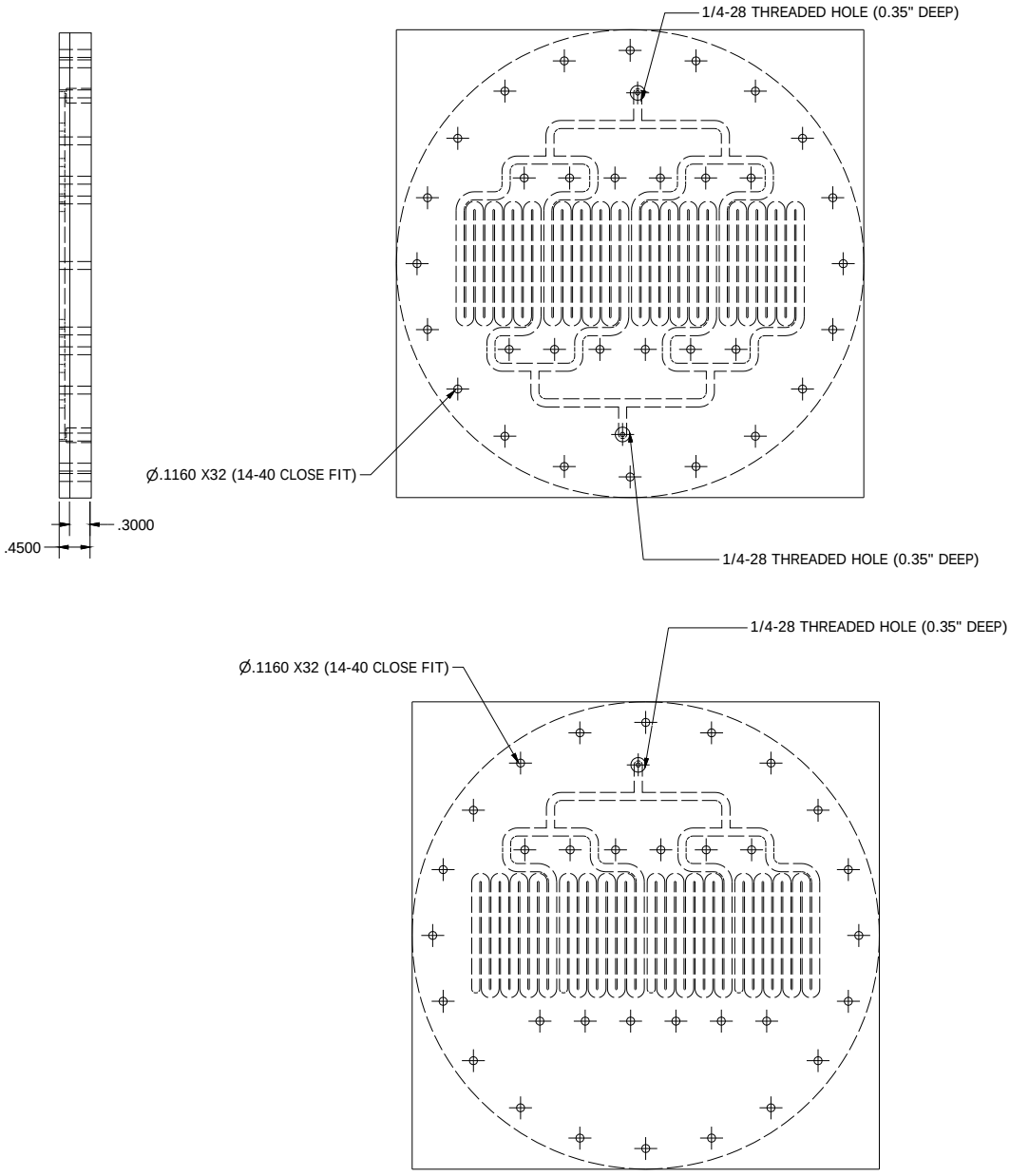

Figure 40. Design 3 drawing. All dimensions given in inches.

(a)

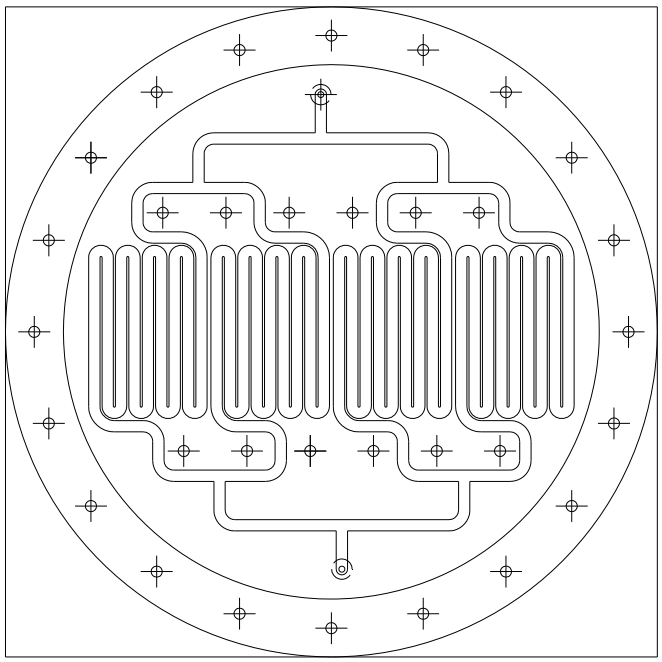

(b)

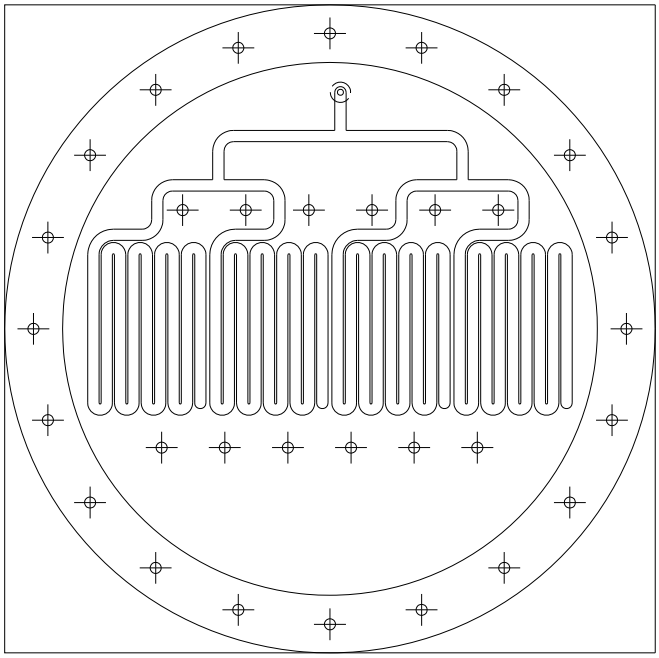

Figure 41. Drawing of channel for (a) retentate and (b) permeate sides of membrane separator. Drawings are at 1:2 scale.

C.4 Design 4

The separators used in the continuous plant are made up of six layers. The top and bottom layers are made of stainless steel and provide the threaded connections and structural rigidity to clamp the device together. Figure 42 shows the drawing of the top and bottom parts.

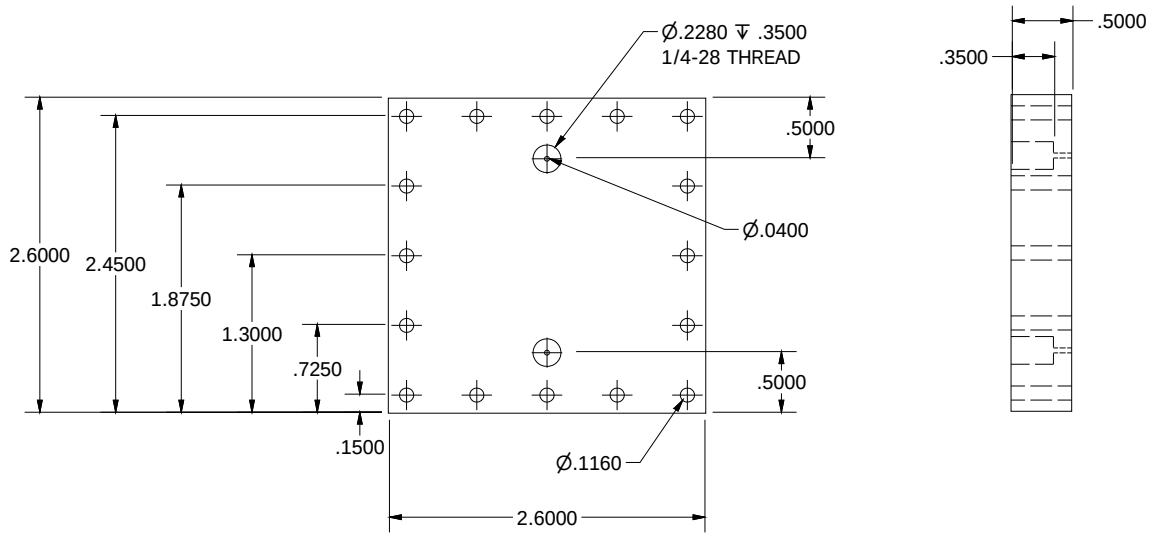

Figure 42. Drawing of top and bottom plate for membrane separator. All dimensions given in inches.

The channel itself is entirely PTFE, made up of 1.59 mm thick sheets of PTFE which are cut using a waterjet and clamped between the top and bottom plates. The top and bottom metal plates are identical, but one side only requires one port. This is achieved by using two different top channels with one having both holes cut (retentate side), and one having only a single hole cut (permeate side).

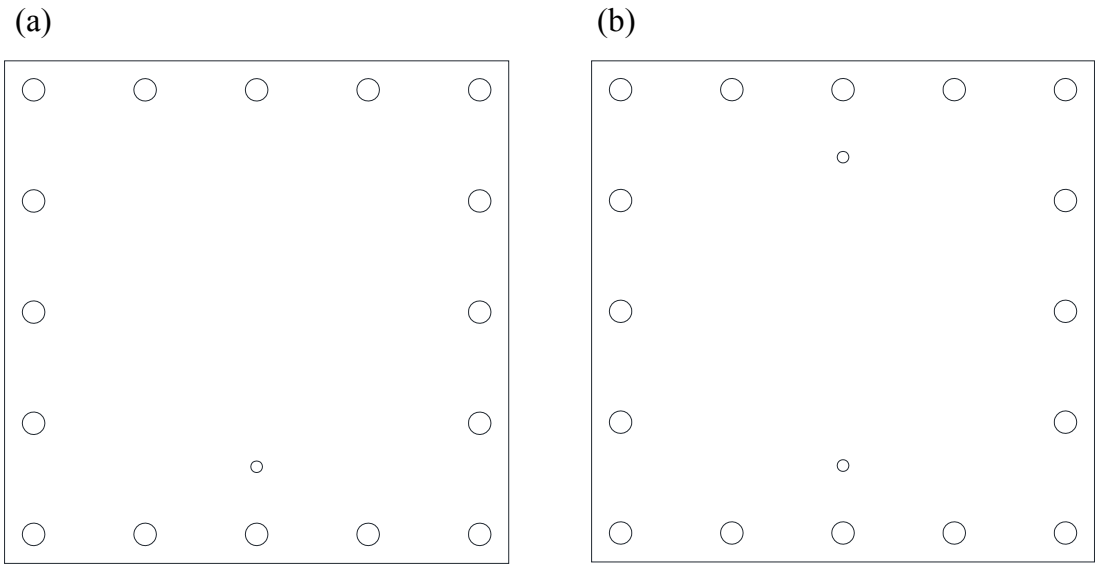

Figure 43. (a) Permeate side PTFE channel top. (b) Retentate side PTFE channel top. Parts are drawn to scale.

The channels are identical and consist of a single sheet of PTFE on each side of the membrane with the channel cut through it. Figure 44a shows the complete channel with a large circle indicated the position of the 47 mm diameter microfiltration membrane. Cutting the entire channel in one pass results in the long, thin channel walls moving and while cutting and the channel geometry ends up deformed or walls are removed entirely. This is solved by introducing tab into the part when cutting (Figure 44b). The tabs secure the walls separating the channels and are easily removed with a razor blade after the part is cut with the water jet. The last layer is the microfiltration membrane which is placed in the middle between the two channel layers.

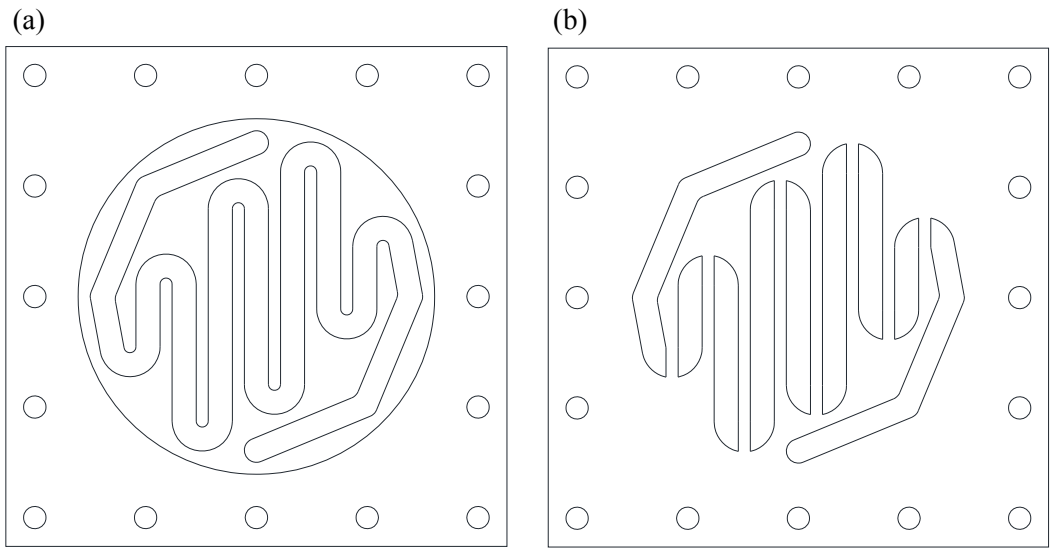

Figure 44. (a) Channel drawing with membrane location shown by large circle. (b) Channel with tabs to hold walls of channel during water jet cutting. Parts are drawn to scale.